5-2014

DETERMINATION OF PORE SIZE DISTRIBUTION IN CAPILLARY-CHANNELED POLYMER (C-CP) FIBER STATIONARY PHASES BY INVERSE SIZE-EXCLUSION CHROMATOGRAPHY (ISEC) AND THE STUDY OF THE ROLE OF INTERSTITIAL FRACTION ON C-CP FIBERS ON PROTEIN BINDING CAPACITY

Zhengxin Wang
Clemson University, zhengxw@g.clemson.edu

DETERMINATION OF PORE SIZE DISTRIBUTION IN CAPILLARY-CHANNELED POLYMER (C-CP) FIBER STATIONARY PHASES BY INVERSE SIZE-EXCLUSION CHROMATOGRAPHY (ISEC) AND THE STUDY OF THE ROLE OF INTERSTITIAL FRACTION ON C-CP FIBERS ON PROTEIN BINDING CAPACITY

A Dissertation
Presented to
the Graduate School of
Clemson University

In Partial Fulfillment
of the Requirements for the Degree
Master of Science
Chemistry

---

by
Zhengxin Wang
May 2014

Accepted by:
Dr. R. Kenneth Marcus, Committee Chair
Dr. Jeffery Anker
Dr. Brian Dominy

ABSTRACT

High performance liquid chromatography (HPLC), first used in the 1960's, is a rapidly evolving analytical technique, widely employed for identification, separation, and purification in biotechnology and pharmaceutical industries. The development of the stationary phases has played an important role in improving this technique. Each stationary phase will have its own disadvantages. Polysaccharide-based stationary phases such as cross-linked dextran cannot tolerate high pressures and linear velocities; silica stationary phases are rigid enough but slow mass transfer in the pores on the surface causes another problem; with the introduction of non-porous and small bead packing materials, the low surface area and high backpressure still handicapped people from achieving better separations. Therefore, fiber based polymer stationary phases came into view.

Capillary-channeled polymer (C-CP) fibers have been investigated in the Marcus laboratory for several years as a stationary phases for ion-exchange (IEC), reversed phase (RP), and hydrophobic interaction (HIC) chromatography. When packed into a column, the unique eight-channeled shape makes them interdigitate to form parallel channels with high surface area-to-volume ratio and low backpressure. Additionally, C-CP fibers are *virtually* non-porous toward large molecules, which decreases the mass transfer to achieve fast protein separations.

In the first study, polypropylene (PP) C-CP fibers and inverse size exclusion chromatography (iSEC) were employed to determine the pore size distribution

(PSD) on the surface of the fibers. With the findings of mean pore size radius and standard deviation, the fibers' geometric structure and adsorption behavior is better understood. In the second study, with the evaluation of the effects of different factors such as interstitial fraction and flow rate on the loading capacity of nylon-6 fibers, the kinetic and thermodynamic properties of the fibers have been further revealed. All results presented the potential of C-CP fibers as an innovative stationary phase for fast macromolecule separations.

DEDICATION

This dissertation is dedicated to all those who believed in me with endless love, patience, and encouragement.

To my parents that always start out conversations with “Are you OK there?”, and end them by saying “How much money you need?”. I know how much you love me, but the thousands words and endless missing are too heavy to pass through the phone over the ocean, which eventually become only several simplest greetings.

To my girlfriend, Liwen, who has never showed up here, but is forever in my mind and heart. Thank you for your unwavering support, patience, and endless love. I’ll be with you soon and to stay.

To my grandmother who is in heaven now. Thank you for using infinite affection and profound enlightenment to fill my childhood so that I could step towards my goals with determination for the rest of my life.

ACKNOWLEDGEMENTS

First I must thank my research advisor, Dr. Marcus, for providing me the opportunity of doing research in his laboratory. Thanks for his responsibility, support, and patience with an international student. Thanks for his guidance, suggestions, and refinements of my research. In addition to his instructions on my research, his charming personality and strong principles also helped me grow during my time here.

I would like to thank past and present members of the Marcus group for their patience, friendship, and support. Thanks to Abby, Marissa, and Ben for tolerating my language skills, helping with my research, and revising my papers. Thanks to Lynn and Daniel for being huge help on my life in a foreign country.

I would also like to thank Dr. Anker and Dr. Dominy for their instruction on my research and literature talk as well as Barbara for the guidance during my TA career.

This material is based upon work supported by the National Science Foundation Division of Chemistry under Grant No. 1011820 (co-funded by the MPS/CHE, ENG/CBET, and EPSCoR).

TABLE OF CONTENTS

Page

Table of Contents (Continued)

Page

LIST OF TABLES

Table Page

LIST OF FIGURES

List of Figures (Continued)

Figure Page

List of Figures (Continued)

Figure Page

CHAPTER ONE

INTRODUCTION

Introduction to Liquid Chromatography

Chromatography is an important branch of analytical chemistry, has been wildly used in the identification, separation, and purification of biomolecules in biotechnology and pharmaceutical industries. Liquid chromatography (LC) is credited to Russian botanist Mikhail Tswett and his famous experiment of separating colored pigments dissolved in pure petroleum ether and run through a chalk column [1,2]. In classic chromatography, large-diameter glass tubes packed with large porous stationary phases were commonly utilized and gravity was the only driving force to let the mobile phase run through the column, which resulted in the disadvantages of slow mass transfer of the analytes, low column efficiency, and tedious separation. High pressure liquid chromatography (HPLC) was named in contrast with the classic chromatography with low pressure and was developed in the 1970's [3]. The substitution of pumps for gravity as the driving force in HPLC significantly increased the separation efficiency, especially after it was found that small packing materials could achieve better separation. As the further realization of both theory and practice of chromatography, it was found that pressure was not the only crucial issues of the process, "high performance liquid chromatography" gradually became a more universal term for HPLC [4]. Over the years research has been devoted to developing different types of chromatography, innovating

stationary phases to achieve better separations, and also developing better detectors, auto samplers, and data systems to continuously improve the chromatographic system.

Theory of Chromatography

In HPLC, a liquid sample with several components is driven by pump force to flow through a column packed or fused with stationary phase. When various components pass through a column, different interactions between components and stationary phase result in different retention times (t_R) from the inlet to outlet of the column. Retention times are usually normalized by the introduction of capacity factor or retention factor (*k*) which is presented as Eq. 1.1: [4,5]

$$k = \frac{t_R - t_0}{t_0} \qquad \text{Eq. 1.1}$$

where t_0 is the deadtime of the system determined by the retention time of analytes unretained in the column. Additionally, the various components form bands when they migrate through the column because of the pressure, resulting in a sequence of chromatographic peaks with different retention times and widths (*w*) which can be detected and recorded by using detectors and data systems.

The goal of using chromatography is to sequence or separate different components of a mixture in a short time and with high resolution. Resolution (R_s) is an important parameter to determine the degree of separation of two chromatographic peaks and is defined as Eq. 1.2: [4,5]

$$R_s = \frac{2(t_2 - t_1)}{w_2 + w_1} \qquad \text{Eq. 1.2}$$

where w_1 and w_2 are peak widths of peaks with retention time of t_1 and t_2, correspondingly. As it is shown in Eq. 1.2, the Δt can be easily increased by increasing the length of column to improve the resolution, however, the peak widths will also increase because of the diffusion, which reduces the practicability of this method. Therefore, a column with higher efficiency which can perform better separation per unit length to form narrower peaks is desired. To better determine the column efficiency, the plate theory and two parameters of theoretical plates number (N) and the height equivalent to a theoretical plate (HETP or H), were introduced by Martin and Synge in 1941 which can be defined by Eq. 1.3 and 1.4: [4,5]

$$N = 16\left(\frac{t_R}{w}\right)^2 \qquad \text{Eq. 1.3}$$

$$H = \frac{L}{N} \qquad \text{Eq. 1.4}$$

where L is the length of column. In 1959, van Deemter further developed the plate theory and described the relationship between HETP and linear velocity under the circumstance of packing, diffusion, and mass transfer, which is presented as Eq. 1.5 and Fig. 1.1[4-6]

$$H = A + \frac{B}{u} + Cu \qquad \text{Eq. 1.5}$$

where *u* is linear velocity, the A term is eddy diffusion term, which is a constant based on the packing condition of column and independent of linear velocity. Eddy diffusion is created by analytes passing through the column by various paths, resulting in band broadening [7]. To minimize eddy diffusion, small size of particles and homogenous packing of stationary phases are necessary (also the electroosmotic driven capillary electrochromatography significantly prevents the stream from being Laminar flow, resulting in extremely low A term [8]). B term is longitudinal diffusion term, which is caused by the analytes' trend of dispersion to every direction due to the concentration gradient [6,9].

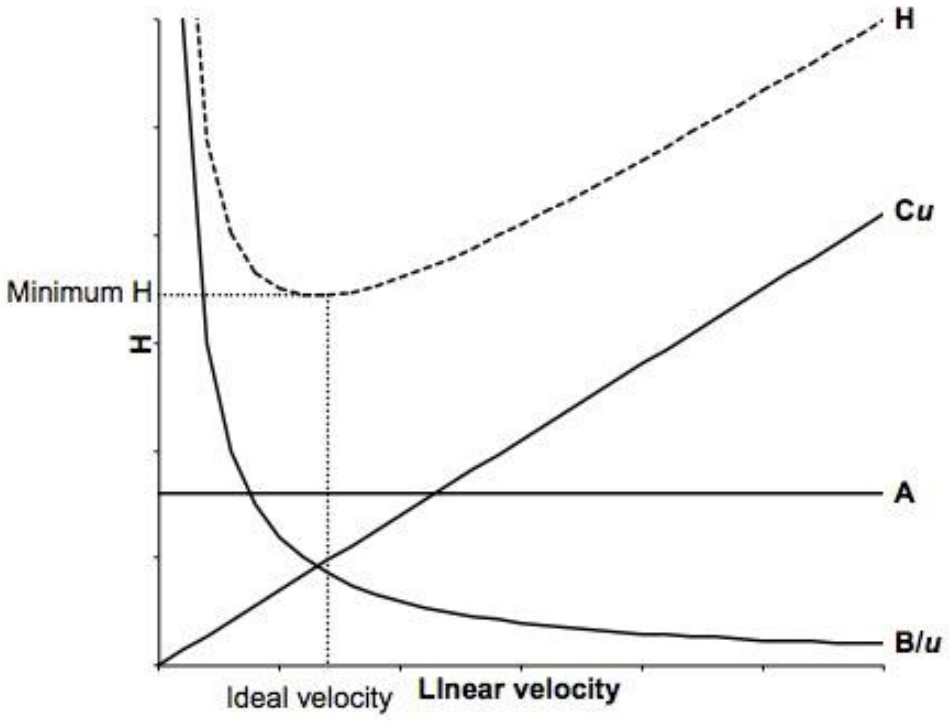

Figure 1.1. The van Deemter plot illustrating the different terms' contribution to band broadening

The B term can be minimized by choosing optimum mobile phase and appropriate concentration of analyte to decrease the analyte diffusion coefficient in it, or using short and narrow column with non-porous packing materials to decrease the obstructive factor. The C term represents mass transfer, which is the sum of several factors ($C = C_m + C_s$) [6,10]. First, if the stationary phase is porous, the band broadening is caused by different degrees of analyte penetration into the pores which occurs only in the stagnant mobile phase within pores by diffusion (C_m). This term can be depressed by using small or non-porous packing materials. Second, in the case of partition chromatography, band broadening is caused by the difference in speeds of varying analytes to enter and escape the interior and surface of small units of adsorbing liquid by diffusion ($C_{s\ partition}$). Third, band broadening due to adsorption chromatography, results from the kinetic process of molecules' different speeds of transportation between two phases due to the sorption-desorption ($C_{s\ adsorption}$). Additionally, C term dominates the high linear velocity zone, decreasing flow rate can also significantly minimize the band broadening. Over the years, Knox [11] and Snyder [3] also made contributions in refining van Deemter equation.

Protein Separations and Stationary Phases

Proteins express the functions of biological cells in any living being. Protein separations are required by both biotechnology and pharmaceutical industry [12]. Additionally, with the increasing dose requirement of pharmaceutical grade protein

per patient and the switch of gene expression system from fungus to human cells to achieve higher homogeneity, both the proteins' productivity and purity are desired in the modern pharmaceutical industry. Protein separations faced big challenges even from their origin in the 1950's – there are more than 20,000 proteins coded by the human genome [12], a protein sample harvested from human cell expression system contains numerous kinds of proteins and peptides. People never stopped developing methods of protein separations, which innovated several widely used techniques so far, including immunoassays [13], gel electrophoresis [14], chromatography [15], membrane-based techniques [16] and more.

The types of chromatography applied in protein separations include ion-exchange chromatography (IEC) [17], reversed-phase chromatography (RPC) [18], hydrophobic interaction chromatography (HIC) [19], and size exclusion chromatography (SEC) [20]. Ion-exchange chromatography (IEC) is widely employed in commercial protein separations as the first step because of its high capacity and low expense. In IEC, the separation is achieved based on the different binding strengths between analytes with different electrostatic charges and stationary phase (ion exchanger) with oppositely charged ionic functional groups [21]. Since the first time IEC was used to separate large molecules in 1954 [15], new stationary phases for IEC have been continuously created. In general, the innovative stationary phases which can solve problems such as the stability,

mass transfer, loading capacity, and back pressure still create a huge space improving this technique.

The capillary-channeled polymer (C-CP) fibers have shown good performance as HPLC stationary phases for protein separations in IEC, RPC, and HIC [22-24] modes in this laboratory. C-CP fibers such as polypropylene (PP), nylon-6, and polyester (PET) have their unique structures of eight-channeled shape (see Fig. 1.2a). Because of this unique structure, C-CP fibers will interdigitate when packed into a column (see Fig. 1.2b), yielding a monolithic-type structure of parallel channels with high surface area-to-volume ratio and low backpressure [25-27].

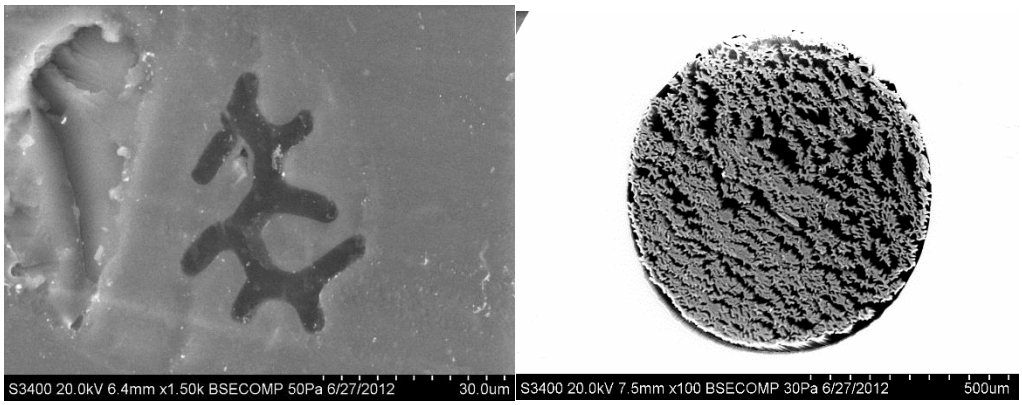

Figure 1.2. a) SEM image of cross section of a PP fiber, b) SEM image of cross section of a PP fiber packed column.

Because of the different chemical functional groups, some polymers such as nylon-6 can be both anion and cation exchangers for IEC under different pH conditions [28]. Advantageously, C-CP fibers are *virtually* non-porous for large molecules,

which significantly decreases the mass transfer term so as to achieve fast protein separations.

Summary

The focus of the work presented in this thesis is based on the determination of pore size distribution (PSD) in PP C-CP fibers and loading capacity of nylon-6 C-CP fibers with the influence of several factors. Chapter two is about using inverse size exclusion chromatography (iSEC) to determine the PSD of PP fibers. A set of probes with different hydrodynamic radius was utilized to generate response curve. By fitting the response curve into the Gaussian and log-normal distribution equations, the mean pore radius and standard deviation were determined. Also, van Deemter plots were employed to verify the non-porous structure of PP fibers with the lack of mass transfer term.

Chapter three describes how the loading capacity of nylon-6 fibers is influenced by different column interstitial fractions and flow rates by employing frontal analysis (FA). 5 columns with different packing densities were utilized to measure the loading capacities of BSA under different flow rates. Batch equilibrium studies and batch dynamic studies were also used to provide equilibrium and dynamic isotherm of BSA. With the analysis of breakthrough curves and comparison between equilibrium / dynamic isotherm, and equilibrium / dynamic loading capacity, the C-CP fibers' kinetic and thermodynamic properties are better characterized.

References

[1] M. Tswett, Travl. Soc. Naturalistes Varisovic, 1903.

[2] M. Tswett, Ber. Deut. Botan. Geo., 1906.

[3] L.R. Snyder, J.J. Kirkland, J.W. Dolan, Introduction to Modern Liquid Chromatography, John Wiley & Sons, Inc., Hoboken, New Jersey, 2011.

[4] R.L. Cunico, K.M. Gooding, T. Wehr, Basic HPLC and CE of Biomolecules, Bay Bioanalytical Laboratory, Richmond, CA 1998.

[5] U.D. Neue, HPLC columns: Theory, Technology, and Practise, Wiley-VCH, New York, 1997.

[6] J.C. Giddings, Unified Separation Science, John Wiley & Sons, INC, New York, NY, 1991.

[7] S.J. Hawkes, J. Chem. Educ, 60 (1983) 393.

[8] M.M. Dittmann, G.P. Rozing, J. Chromatogr. A, 774 (1996) 63.

[9] J.H. Knox, H.P. Scott, J. Chromatogr. A, 282 (1983) 297.

[10] A.M. Siouffi, J. Chromatogr. A, 1126 (2006) 86.

[11] J.H. Knox, J. Chromatogr. A, 15 (1977) 352.

[12] D.A. Egas, M.J. Wirth, Annu. Rev. Anal. Chem., 1 (2008) 833.

[13] R.S. YALOW, S.A. BERSON, Nature, 184 (1959) 1648.

[14] K. Weber, M. Osborn, J. Biol. Chem., 244 (1969) 4406.

[15] E.A. Peterson, H.A. Sober, Fed. Proc., 32 (1954) 273.

[16] J.T. Lawhon, L.J. Manak, K.C. Rhee, E.W. Lusas, J. Food Sci., 46 (1981) 391

[17] S. YAMAMOTO, K. NAKANISHI, R. MATSUNO, T. KAMIKUBO, Biotechnol. Bioeng., 25 (1983) 1465.

[18] K. UNGER, G. JILGE, J. KINKEL, M. HEARN, J. Chromatogr. A, 359 (1986) 61.

[19] S. Xie, F. Svec, J.M. Fréchet, J. Chromatogr. A, 775 (1997) 65.

[20] W. Kopaciewicz, F.E. Regnier, Anal Biochem., 126 (1982) 8.

[21] D. Sheehan, R. FitzGerald, Methods Mol. Biol., 59 (1996) 145.

[22] R.K. Marcus, W.C. Davis, B.C. Knippel, L. LaMotte, T.A. Hill, D. Perahia, J.D. Jenkins, J. Chromatogr. A, 986 (2003) 17.

[23] R.D. Stanelle, R.K. Marcus, Anal. Bioanal. Chem., 393 (2009) 273.

[24] A.J. Schadock-Hewitt, J.J. Pittman, K.A. Stevens, R.K. Marcus, J. Appl. Polym. Sci., 128 (2013) 1257.

[25] R.D. Stanelle, L.C. Sander, R.K. Marcus, J. Chromatogr. A, 1100 (2005) 68.

[26] K.M. Randunu, S. Dimartino, R.K. Marcus, J. Sep. Sci., 35 (2012) 3270.

[27] J.M. Randunu, R.K. Marcus, Anal. Bioanal. Chem., 404 (2012) 721.

[28] R.D. Stanelle, C.A. Straut, R.K. Marcus, J.Chromatogr. Sci., 45 (2007) 415.

CHAPTER TWO

DETERMINATION OF PORE SIZE DISTRIBUTIONS IN CAPILLARY-CHANNELED POLYMER (C-CP) FIBER STATIONARY PHASES BY INVERSE SIZE-EXCLUSION CHROMATOGRAPHY (ISEC) AND IMPLICATIONS FOR FAST PROTEIN SEPARATIONS

Introduction

High performance liquid chromatography (HPLC) plays a crucial role in the identification, characterization, and processing of proteins, ranging in scale from chip-based proteomics studies to the industrial scale in biotechnology and pharmaceutical applications [1,2]. Numerous new packing materials, including organic and inorganic polymers, have been introduced as stationary phases to improve biomolecule separation quality [3]. While exquisite surface chemistries have been developed to affect high levels of chemical selectivity, the chromatographic efficiencies, throughput, and binding capacities of a system are dictated by the physical characteristics of a given phase. High levels of porosity within small particles provide for bed uniformity, short diffusion distances, and large phase ratios, leading to enhanced efficiencies for small molecule separations; but mass transfer limitations hinder their utility for macromolecule applications. Preparative macromolecule separations are met with the conflicting metrics of high equilibrium binding capacities of porous media, versus their low processing rates/throughput.

Virtually all chromatographic packing materials (i.e., support phases) have porosity on some level. As both the geometry and density of pores can affect the adsorption of analytes and transport behavior of fluid flow, characterization of the pore structure of new chromatographic packing materials is necessary for all candidate stationary phases, with regards to the particular application at hand [4]. The pore size distribution (PSD) of a given stationary phase reflects the density of pores within a certain radii range, making it a critical parameter in describing pore structures [5]. Several methods can be used to determine the PSD of a stationary phase, including mercury intrusion [6], nitrogen adsorption [7], atomic force microscopy [8], and more recently, ellipsometric porosimetry [9]. Of greater practical relevance, inverse size exclusion chromatography (iSEC) is commonly used because it probes the material under chromatographic conditions [10-12].

iSEC has several advantages in comparison to the other methods. For example, in mercury intrusion and nitrogen absorption determinations, a dry experimental environment with high pressure and low temperature are necessary [6,7], which would cause the structural damage of some materials such as polymer beads. In iSEC, intact structural information of materials can be achieved without morphological changes. In addition, iSEC is operated under typical chromatographic conditions, so it is a relatively convenient and inexpensive approach [5]. The method is a simple variation of the size-exclusion chromatography (SEC), used to entropically separate macromolecules based on their hydrodynamic volume or relative size [13]. In SEC, solutes of unknown

size/molecular weight (MW) are sequenced using a packing material of known pore dimensions. Conversely, iSEC uses molecules of known size to determine the packing material's unknown pore dimensions [10].

The technique of iSEC was first utilized by Aggerbrandt and Samuelson in 1964 [14] to determine the pore size distribution (coincidently) of cellulose fibers. Later, Knox [15]and Svec [16]made substantial contributions to refine and apply the theory. With the mathematical models established by Gorbunov in 1988, both the theory and practice of iSEC was strengthened and extended [17]. Yao and Lenhoff have presented an excellent review of the methodology [5]. In the basic experiment, a set of probe species having different hydrodynamic radii (r_m) are injected into a HPLC system to determine their retention times (t_r) and volumes (V_e) under mobile phase conditions which they are not enthalpically retained (i.e., non-retaining conditions). In iSEC, as in SEC, the large molecules are excluded from the pores and therefore elute first, as small molecules become entrapped in the pores of the stationary phase to various extents and elute later. The operational aspects of iSEC are presented in Fig. 2.1 where V_0 is indicative of the column void volume obtained by the retention volume of a solute too large to penetrate the pores, and V_t is the total permeable volume of the column obtained from the retention volume of the solute that is retained for longest time (presumably the smallest r_m). Solutes of intermediate hydrodynamic radii elute at corresponding retention times.

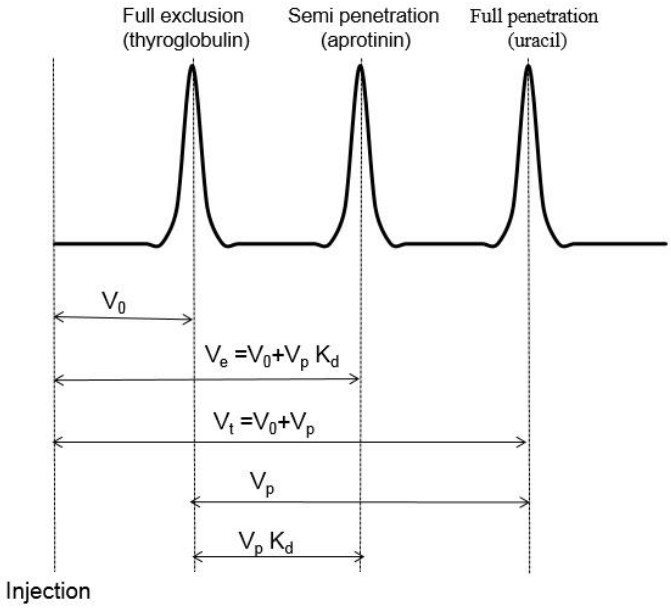

Figure 2.1. Extraction of iSEC parameters from the retention volumes (V_e) of probes having different hydrodynamic sizes.

The distribution coefficient, K_d, also called the partition coefficient [18,19] or the exclusion coefficient [15], represents the fraction of the pore volume accessible to the various solutes and ranges from zero to unity [20]. Chromatographically, this can be calculated by Eq. 2.1 [21]:

$$K_d = \frac{V_e - V_0}{V_t - V_0} \qquad \text{Eq. 2.1}$$

In iSEC, the response curve of K_d vs r_m graphically provides important information about the PSD. Ideally, the pores in a given material are assumed to be of the same shape, but having different geometric cross-sections [21]. The pore size distribution function f(*r*) represents the pore cross-section dimensions, thus the total pore volume whose cross-section is in the range between pore radius (*r)* and

r+d*r* can be calculated. A Gaussian function is commonly used to model the PSD, with the PSD function presented as:

$$f(r) = \exp\left[-\frac{1}{2}\left(\frac{r-r_p}{s_p}\right)^2\right] \qquad \text{Eq. 2.2}$$

where r_p is mean pore radius and s_p is standard deviation of the distribution.

While the Gaussian distribution is mathematically straight forward, there are occasions where it provides negative range of r values in distribution, which of course have no physical meaning. To avoid the negative distribution in the lower range of r-values, a log-normal distribution has been used [21,22]:

$$f(r) = \frac{1}{\mathrm{r}}\exp\left[-\frac{1}{2}\left(\frac{\log(\mathrm{r}/\mathrm{r_p})}{\mathrm{s_p}}\right)^2\right] \qquad \text{Eq. 2.3}$$

where r_p and s_p have less physical meaning than the Gaussian distribution, but still represent the centroid of the distribution and breadth respectively. Use of a log-normal representation of retention data (log molecular weight/molecular radius vs retention volume) is a very common means of visualizing the size cut-off characteristics of porous phases [5,10,23,24]. In this work, both of the methods will be presented so as not to pre-suppose the actual pore size distribution function.

The interpretation of K_d in a separation is model-dependent realizing that neither probe molecules nor the probes can be adequately described mathematically in four dimensions. The most generic description, a spherical

probe in a cylindrical pore, is used here, so the distribution coefficient for a single pore, K, is presented as [15]

$$K = \left(1 - \frac{r_m}{r}\right)^2 \qquad \text{Eq. 2.4}$$

Integrated and normalized across the probe and pore populations, the accessible pore volume is presented by the Gaussian distribution [21]

$$K_d = \frac{\int_{r_m}^{\infty} f(r)Kdr}{\int_0^{\infty} f(r)dr} = \frac{\int_{r_m}^{\infty} e^{-\frac{1}{2}(\frac{r-r_p}{s_p})^2}(1-\frac{r_m}{r})^2 dr}{\int_0^{\infty} e^{-\frac{1}{2}(\frac{r-r_p}{s_p})^2} dr} \qquad \text{Eq. 2.5}$$

and is further described by the log-normal distribution [21]

$$K_d = \frac{\int_{r_m}^{\infty} f(r)Kdr}{\int_0^{\infty} f(r)dr} = \frac{\int_{r_m}^{\infty} \frac{1}{r} exp\left\{-\frac{1}{2}\left[\frac{log(r/r_p)}{s_p}\right]^2\right\}\left(1-\frac{r_m}{r}\right)^2 dr}{\int_0^{\infty} \frac{1}{r} exp\left\{-\frac{1}{2}\left[\frac{log(r/r_p)}{s_p}\right]^2\right\} dr} \qquad \text{Eq. 2.6}$$

By fitting the response curve of K_d vs r_m obtained from Eqn. 1 into model Eqns. 2.5 and 2.6, the r_p and s_p can be determined.

iSEC has been successfully applied in the determination of the porosities of several packing materials [4,5,10-12,25]. In this work, iSEC is used to determine the PSD of capillary-channeled polymer (C-CP) fibers [26]. C-CP fibers have been utilized as combined support/stationary phases for protein separations in this laboratory in ion-exchange (IEC), reversed phase (RP), and hydrophobic interaction (HIC) chromatography modes [26-28]. Figure 2.2 is a cross-sectional image of a polypropylene (PP) C-CP fiber taken by scanning electron microscopy.

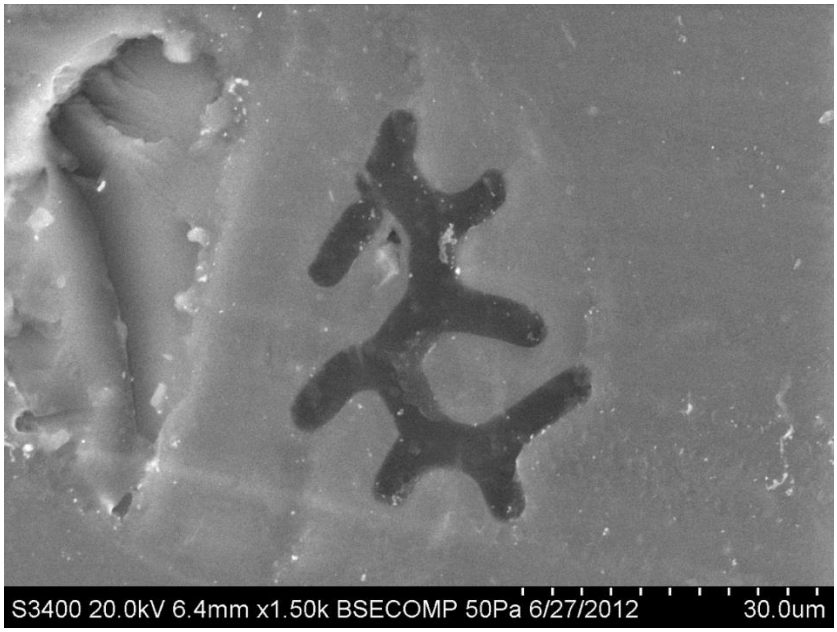

Figure 2.2. Cross sectional scanning electron micrograph of the polypropylene C-CP fibers used in this work.

The eight capillary channels of the fiber and the well-defined channel walls are well presented in the micrograph. Due to the eight-channeled shape, PP C-CP fibers have a larger (~3x) surface area-to-volume ratios than circular cross section fibers of the same nominal diameter, with specific surface areas that are comparable to monolithic phases (single m^2 g^{-1}) [26]. This shape also allows the fibers to interdigitate when packed in a column structure, yielding a monolithic structure of parallel channels [29-31]. Because of the collinear nature of the fibers, high mobile phase linear velocities (>100 mm s^{-1}) can be achieved at modest backpressures (<2000 psi). Advantageously, C-CP fibers have a unique feature: an actual improvement in chromatographic resolution for biomacromolecules as linear velocity is increased [31]; implying no van Deemter C-term limitations. This

phenomenon provides the ability to perform very fast analytical separations [31,32] and achieve high throughputs and yields in preparative situations [33]. Based on these merits and very low materials costs, it is envisioned that the C-CP fibers could be applied in process protein separations.

It is easy to assume that the high mass transfer efficiencies suggested above are due to the porosity (or lack thereof) of the individual C-CP fibers. Therefore, a detailed evaluation of the porosity of the fibers is necessary to better understand this material; iSEC is the ideal approach to that end. In this work, a set of probes species having different hydrodynamic sizes (and chemistries) have been employed. In many other works, a series of homologous polymers (e.g., polysaccharides) has been employed to normalize potential enthalpic contributions to retention while having similar three-dimensional shapes [21,34]. Based on the use here of UV-VIS detection, and a desire to more realistically mimic potential protein separations, that approach was not taken; using metal ions, small organics, polypeptides and proteins instead. In order to span the entirety of practical sizes, the test suite included the common marker compound uracil, the inorganic salt $CuCl_2$ (Cu^{2+} in solution), the polypeptides nisin and aprotinin, and the proteins cytochrome C, ribonuclease A, myoglobin, β-lactoglobulin, albumin, transferrin, glucose oxidase, and thyroglobulin. To be clear, this approach is taken under the assumption that each of these species is treated at spherical/globular in shape; which is correct to various extents. Each solute was injected under non-retaining conditions to determine the relationship between K_d and r_m and extracting the PSD.

van Deemter plots were used to verify the results in terms of the realized chromatographic performance based of the fiber porosity and implications relative to executing high speed protein separations. While a lack of porosity has detrimental effects relative to equilibrium binding capacities in preparative separations because of the low surface area, these characteristics bode well in terms of throughput/productivity [33]. By extension, the lack of porosity also contributes to the high yields/recoveries realized in protein separations to this point [35].

Experimental section

Reagents and Chemicals

HPLC grade acetonitrile (ACN) from Millipore (Billerica, MA), HPLC grade methanol from Alfa Aesar (Ward Hill, MA), and sodium chloride (NaCl) from Sigma-Aldrich (Milwaukee, WI), Milli-Q water (18.2 MΩ cm^{-1}) were employed in the preparation of the mobile phase. Each of the 11 probe ions/molecules, uracil, $CuCl_2$, nisin, aprotinin, cytochrome C, ribonuclease A, myoglobin, β-lactoglobulin, albumin, transferrin, glucose oxidase, and thyroglobulin was purchased from Sigma-Aldrich (Milwaukee, WI). Stock peptide and protein solutions were stored at 4 °C. This set of probes was chosen to provide a range of hydrodynamic radii (r_m). For any solute, a range of r_m values can be found, which are dependent on the specific solvent conditions, and so are difficult to use with great certainty. The species, their respective molecular weights, and the r_m values are presented in

Table 2.1. The radii of uracil and Cu^{2+} were found from literature references [36,37]. In the case of the polypeptide nisin, its radius was calculated using the relationship described by Brissová et al., $r_m = 0.051\ MW^{0.378}$ [38], wherein the experimental values for the other test species listed in Table 2.1 were presented as part of the development of that equation.

Table 2.1. iSEC probe species, their molecular weights and computed hydrodynamic radii (r_m).

Name	Mw(Da)	r_m(nm)
Uracil	112	0.227
Cu^{2+}	64	0.325
Nisin	3,300	1.09
Aprotinin	6,700	1.50
Cytochrome C	11,700	1.63
Ribonuclease A	13,700	1.75
Myoglobin	17,000	1.91
β-Lactoglobuline	35,000	2.70
Albumin	66,000	3.62
Transferrin	77,000	3.92
Glucose oxidase	186,000	5.20
Thyroglobulin	670,000	8.6

Chromatographic Column Preparation

Chromatographic columns were prepared by pulling 480 polypropylene (PP) C-CP fibers through 0.76 mm inner diameter (i.d.), 114 cm long PEEK tubing. The PP fibers were extruded in the School of Materials Science and Engineering of Clemson University and the PEEK tubing was purchased from Upchurch Scientific (Oak Harbor, WA). Fibers pulled through the column are parallel-aligned in such a way to affect high permeability and thus low back pressures in comparison to random-packed fiber phases [26]. Micrographs of packed fibers reflect the fact that

the channels of adjacent fibers interdigitate in such a way that 1-5 µm wide flow paths are created [29-31]; somewhat analogous to the throughpore structure of monoliths. Columns were washed sequentially with ACN, methanol, and Milli-Q water to remove any residual anti-static detergent coatings [26]. Under these packing conditions, the column interstitial fraction was determined to be ~61% using uracil as the test compound; as most commonly used is HPLC stationary phase characterizations. As will be seen, use of a protein marker compound in the future is more relevant for macromolecule separations on C-CP fiber columns.

Chromatographic System and Operations

A Dionex (Sunnyvale, CA) Ultimate 3000 with a LPG-3400SD pump, a WPS-3000TSL autosampler, and a VWD-3400 RS UV-Vis absorbance detector was used as the chromatographic system. The Dionex Chromeleon software (Sunnyvale, CA) was used to collect data, Microsoft Excel (Seattle, WA) and MATLAB (Natick, MA) were used to further process the data. Coincidentally, each of the test species produces appreciable absorbance at 216 nm, with chromatograms reported in units of absorbance at that wavelength as a function of time.

Probes and mobile phase preparations

Because iSEC relies on separation based on the hydrodynamic volume/size of the probe species, rather than by enthalpic interactions with the stationary phase, only the ions/molecules having no chemical interaction with the

fibers, in specific solvent systems, can be used as probes. The only enthalpic driving force between these solutes and the PP surface is a hydrophobic interaction. To determine the extent of potential adsorption, equilibrium (static) depletion determinations were performed by monitoring decreases in free solution concentration of each probe in the presence of a bundle of C-CP fibers. Three solvent compositions were evaluated as potential mobile phases: 40% ACN:H_20, 20% MeOH:H_2O, and 1M NaCl, each made with MilliQ water, at solute concentrations of 0.1mg mL^{-1} in each solvent. A Thermo (Madison, WI) Genesys 10-S UV-Vis spectrophotometer was used to test the solution absorbance. The PP C-CP fibers (~28.5 mg) were placed in a 10 mL volume of the proposed elution solvent and allowed to sit for one hour. The change in solution absorbance (at the probe species' λ_{max}) was used to assess the extent of fiber adsorption. None of the probe species showed changes in the optical absorbance in the 20% methanol solution phase; indicating no measurable adsorption to the fiber surface. Therefore, a 20% MeOH:H_2O mobile phase composition was employed to evaluate the entropic retention (hold-up) of the probe species. Important to the study at hand, none of the probe proteins would be expected to undergo appreciable un-folding under these solvent conditions.

Ultimately, the probe ions/molecules were prepared by mixing in the stock mobile phase solution at a concentration of 0.1 mg mL^{-1}. In the case of the iSEC experiments, the probes were injected individually into the HPLC system at 20 μL volumes at a flow rate of 0.2 mL min^{-1}, corresponding to a linear velocity of 10.1

mm s^{-1}, a value on the lower end for C-CP fiber protein separations to allow for greater pore penetration where possible. The column was washed with 100% ACN and Milli-Q water, in sequence, between the individual injections until a stable optical absorbance baseline was realized. Subsequent studies were performed across a range of linear velocities (0.5 – 27 mm s^{-1}) using uracil, aprotinin, and thyroglobulin as the test species, with those data used to generate van Deemter and Knox plots.

Results and Discussion

Solute retention characteristics

The practical aspects of pore size determinations are based on the retention time/volume of each solute under non-retaining conditions. As such, based on the theory of iSEC, larger molecules, such as proteins, elute before probes whose hydrodynamic radii are smaller than the pores in the phase. Fig. 2.3 depicts the elution profiles of the probe ions/molecules at the fixed mobile phase flow rate of 0.2 mL min^{-1}. (The plots are normalized according to each species' maximum absorbance.) Each of the presented transients is the average of three injections, wherein the retention times for the maxima differ by less than 0.5 % RSD for each species. Clearly seen is a grouping of the proteins and polypeptides eluting much earlier than the uracil and Cu^{2+} ion; as expected. Other probe molecules, such as aprotinin and cytochrome C, belong to the semi-penetrating (size selective) probe group, with their retention times falling in the middle. Closer inspection of the

profiles of the proteins indicates an inverse relationship between their respective molecular weights (size) and peak retention times.

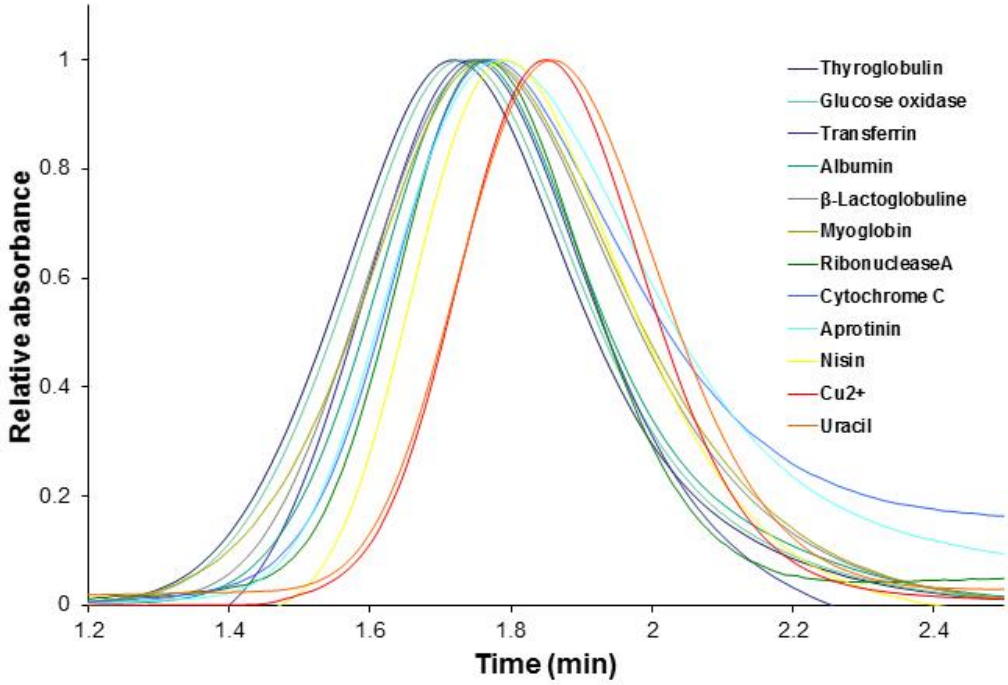

Figure 2.3. Elution profiles of the test probes used the in iSEC experiments. Each transient represents the average of three separate injections. Mobile phase = 20:80 MeOH:H_2O, flow rate = 0.2 mL min^{-1} (u = 10.1 mm s^{-1}).

The response curve of K_d vs r_m (based on the transients of Fig. 2.3) is presented in Fig. 2.4a. Thyroglobulin (the highest mass species) was designated as the fully excluded probe, with its retention volume used as the value V_0 in Eq. 2.1. Uracil was used as the fully penetrating probe, with its retention volume used as V_t. Based on these two retention volumes, the other probes' K_d values were calculated. Because K_d represents the fraction of the pore volume accessible to the solute; the larger the probe, the smaller fraction of the pore volume that is accessible by the solute, and so K_d decreases with increasing probe r_m.

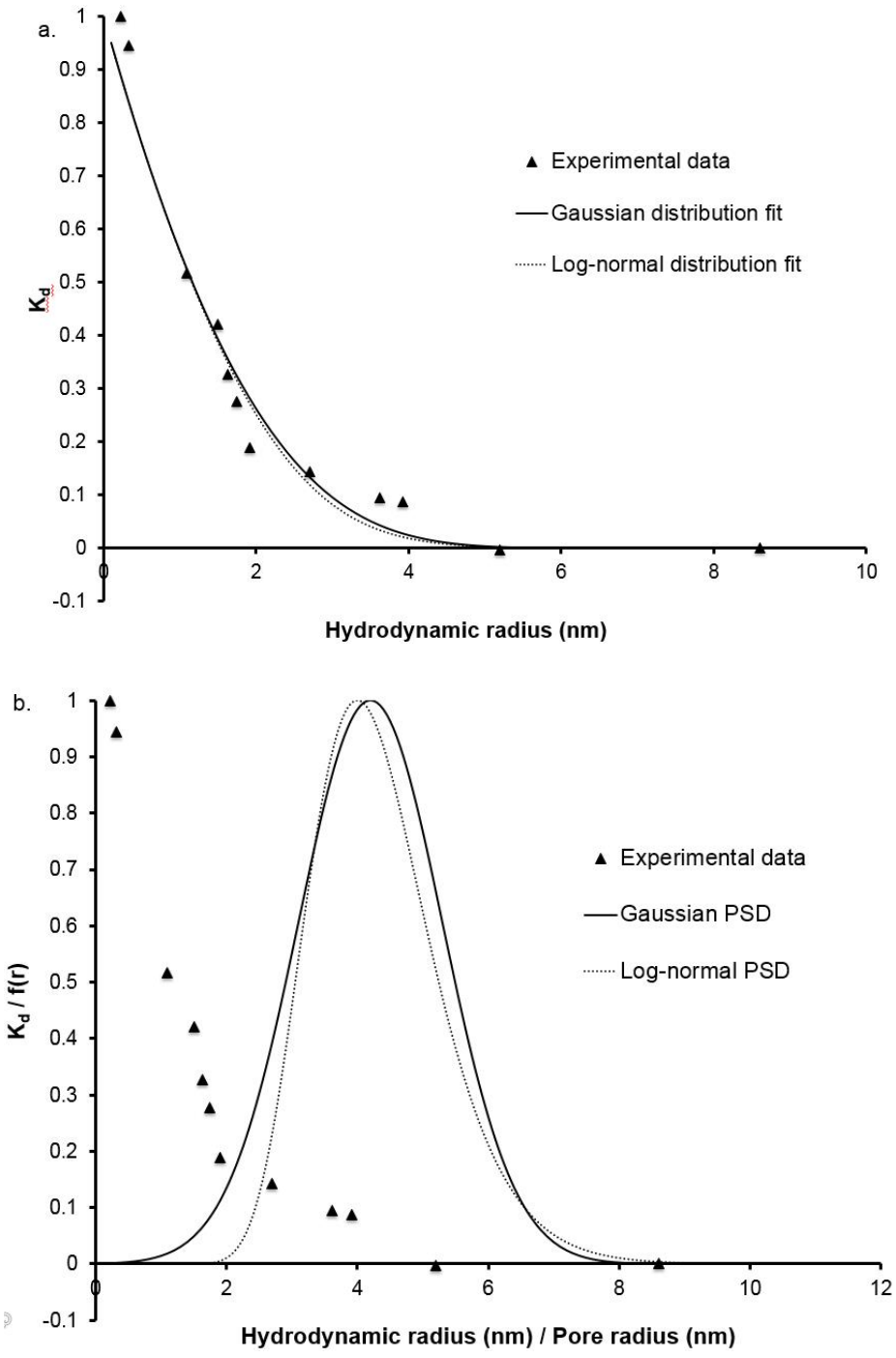

Figure 2.4. a) Response curve and best fittings for Gaussian and log-normal equation. b) The resultant pore size distributions.

There visually appears to be two regions that exist in K_d vs r_m plot. From uracil to myoglobin (r_m = 1.91 nm), the K_d values decrease in an almost linear

fashion with a slope of -0.45 K_d per unit radius in nm. Beyond this point, the curve is comparatively flat, with a slope of -0.036 K_d per unit radius in nm. Shown in Fig. 2.4a as well are the Gaussian and log-normal fits to the experimental data, generated through Eqns. 2.2 and 2.3, respectively. As can be seen, the Gaussian fit tends to be better in the region of the inflection point, with an overall least-squares goodness-of-fit $R^2 = 0.83$, with the log-normal fit yielding and $R^2 = 0.55$. The better fit for the former implies that the distribution of sizes does not exhibit appreciable skew or asymmetry.

A qualitatively-similar response curve to Fig. 2.4a was obtained by Ladisch and co-workers for DEAE-modified cotton:polyester (60:40) yarns using glucose, PEG, and dextran probes [39]. (Unfortunately, the PSD was not calculated in that work.) Even before computational evaluation, it is clear that the molecular sizes to the right of the break point have limited-or-no access to the pores, with the retention volumes being fairly independent of molecule size. The species to the left of the break point are fully and/or semi-penetrating probes, as the retention times vary significantly based on their molecular sizes.

In terms of commercially available formats, C-CP fiber columns are most closely related to monolithic columns in terms of specific surface area and solute/solvent transport properties [40]. It is therefore interesting to compare the relative shapes of the response curves presented in Fig. 2.4a to retention responses published for those phases as this provides some qualitative feel for the pore sizes and their distributions [10,23,24,41]. For example, Guiochon and co-

workers [10] evaluated the PSD of a monolithic Chromolith Performance (Merck) column and a conventional column packed with 10 µm silica particles using polystyrene probe compounds of MW 2000 to 1,861,000 Da, and toluene as the tracer compound. The log MW vs. retention volume in Fig. 1 of that work can be readily converted to the format of Fig. 2.4a here by setting the retention volume of toluene as V_t and that of the highest MW (size) probe as V_0. In doing so, two distinct regions are seen in that data as well, with an inflection point at ~20 nm. The full and/or semi-penetrating probes encompass molecules of 0.9 to 22.8 nm, with a slope of -0.03 K_d per unit radius in nm, much less sensitive to size than the -0.45 K_d per unit radius for C-CP fibers. We interpret the greater sensitivity to size before the exclusion cut-off in Fig. 2.4a here to reflect a smaller average size and greater uniformity of pore size distributions in the C-CP fiber phase. As would be expected, the iSEC data for the particulate column in that work (Phenomenex Luna Prep Silica, 10 µm diameter), reveals a similar distribution, in this case having much lower total porosity than the monoliths [10].

DePhillips and Lenhoff performed perhaps the most thorough evaluation of stationary pore size distributions [21], including silica, methacrylate, and agarose materials employed in cation-exchange separations. As a general rule, the slope of full and/or semi-penetrating probes' part of the response in Fig. 2.4a here is steeper than the same zone in other phases, with the transitions to the excluded species' region appearing at much smaller hydrodynamic radii for the fiber phase.

These basic trends indicate that the pore sizes are more uniformly distributed, at smaller radii, for the PP fiber.

Pore Size Distribution (PSD) of PP C-CP Fibers

The K_d values from the response curve of Fig. 2.4a were fit to Eqns. 2.5 and 2.6 (Gaussian and log-normal functions) using MATLAB routines, with the resulting PSD curves shown in Fig. 2.4b, superimposed on the retention data. Qualitatively, both distributions reflect what would be expected using the basic premise that solute hold-up becomes appreciable as their radii exceed ~10% of the pore radius [1,18] . The respective fits yield a mean pore radius of r_p = 4.2 nm, with a standard deviation of s_p = ± 1.1 nm for the Gaussian distribution and r_p = 4.0 nm, with a standard deviation of s_p = ± 0.1 for the log-normal distribution. The slight bias toward smaller pore sizes for the log-normal fit is expected as it does indeed fit that region of Fig. 2.4a more closely, with the tailing towards the large pore end being equally predictable. The excellent agreement between the average values obtained from the two distribution functions provides confidence in the overall results, with the slightly more narrow breadth of the distribution for the case of the log-normal fit being a product of its logarithmic nature [22].

The mean and standard deviations extracted from the C-CP fiber PSD curves provide a quantitative basis for comparison with other stationary phase materials. Average pore size values presented by DePhilips and Lenhoff [21] for commercially available cation-exchange phases (having methacrylate, silica, and

agarose supports) varied from 6.8 to 68 nm, with relative standard deviations (%RSD = s_d / r_p x 100%) ranging from 1 - 30%; with the vast majority being on the 1-5% level. A subsequent study of PSDs and binding capacities for similar supports, following surface modifications with various polymeric stationary phases, generated values of more of the order of this work, with some showing more narrow breadths [42]; reflecting the filling of the pore structure. Pore size distributions presented by Huber and co-workers for PS-DVB monoliths as well as 2.1 µm diameter bead media generated by iSEC revealed distributions that covered 10s-100s of nm, with maxima in the distributions at ~20 nm for the beads and ~100 nm for the monolithic material [43].

Implications of the PSD as manifest in van Deemter plots

By definition, solid-liquid partition coefficients are driven by the phase ratios realized on a given support, and so greater chromatographic efficiencies are realized through the use of materials of high specific surface area [1]. By the same token, greater surface area, under equilibrium conditions, should translate to greater binding capacities. As a general rule, large specific surface areas are generated through use of high porosity materials. In the case of dynamic separations, particularly of macromolecules of low diffusivity, there becomes a key trade-off between the kinetic and thermodynamic aspects. Thus the pore size distribution characteristics of a support phase affect the binding capacity [42].

Previous works in the characterization of C-CP fiber phases have shown that bed non-uniformity was clearly the limiting feature toward chromatographic efficiency for isocratic separations of small molecules [29,44]. In the context of the van Deemter equation :

$$H = A + B/u + Cu \qquad \text{Eq. 2.7}$$

where H is the theoretical plate height, u is the linear velocity of the mobile phase, A is eddy-diffusion parameter which is related to the column uniformity, B is the longitudinal diffusion coefficient, and C is mass transfer coefficient between mobile and stationary phases [45], C-CP columns are A-term limited. As A-term broadening is by-definition independent of linear velocity in Eq. 2.7, there should be no efficiency-penalty to be paid by using high linear velocities to affect greater throughput and yield so long as there are no mass transfer (C-term) limitations. This is a basic characteristic found in protein separations on C-CP fiber phases [31,32,46].

To better demonstrate the ramifications of the C-CP porosity on potential mass transfer limitations, van Deemter plots were generated for three of the probe species representing the various degrees of pore interaction; uracil for full access, aprotinin for restricted access, and thyroglobulin for full exclusion. As before, the experiments were performed under non-retaining conditions using 20% MeOH:H_2O as the mobile phase. The solution flow rates were varied across a range of 0.01 - 0.5 mL min^{-1} (equating to linear velocities of 0.5 – 27 mm s^{-1}). The

resultant van Deemter plots for the three probe molecules are presented in Fig. 2.5, with the solid lines representing the least-squares fitting. Each of the data points in the plot represents the average of 3 individual solute injections, with the average variation under a given set of conditions being on the order of 0.4 %RSD. The table presents the derived A, B and C-term values after fitting the experimental data to Eq. 2.7.

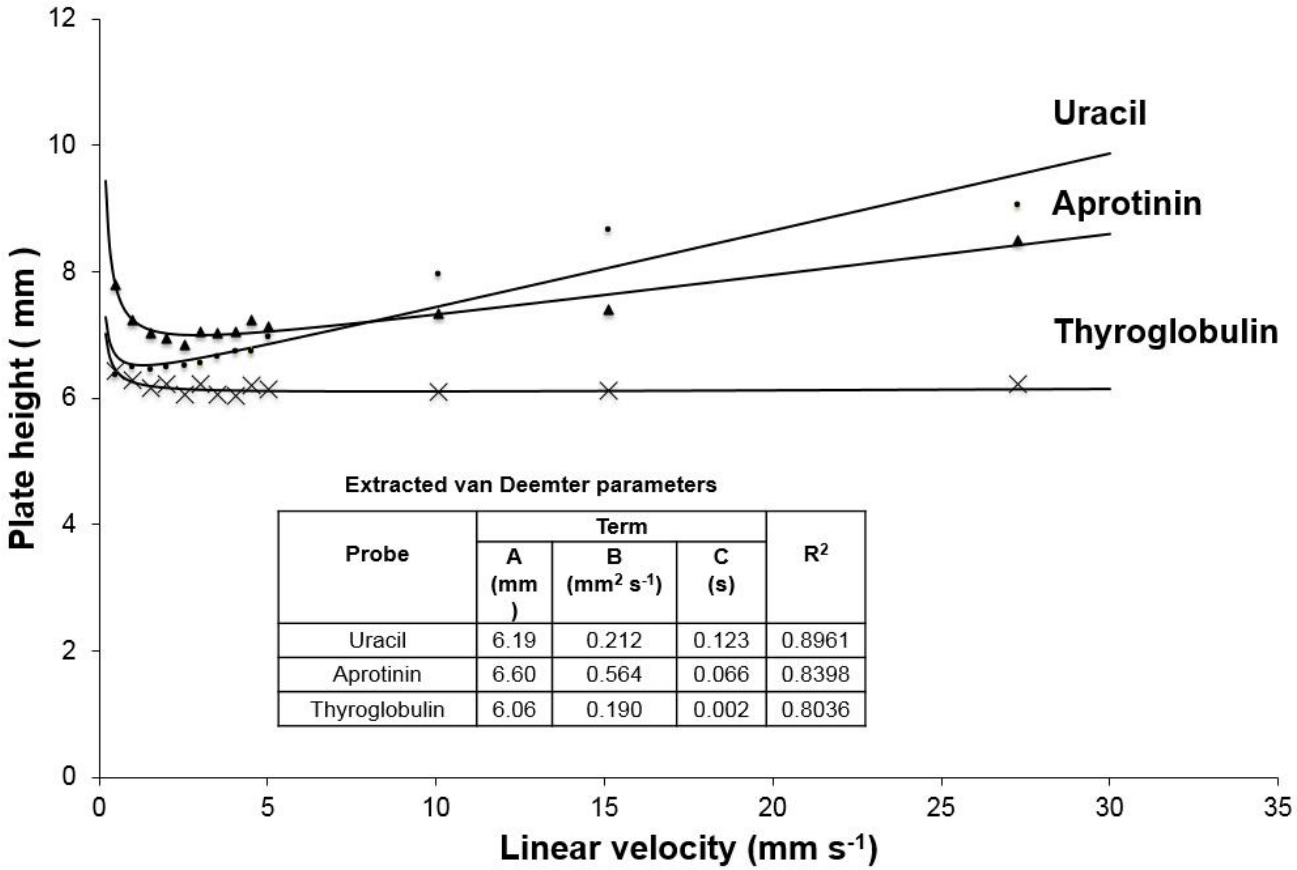

Extracted van Deemter parameters

Probe	Term			R^2
	A (mm)	B ($mm^2\ s^{-1}$)	C (s)	
Uracil	6.19	0.212	0.123	0.8961
Aprotinin	6.60	0.564	0.066	0.8398
Thyroglobulin	6.06	0.190	0.002	0.8036

Fig. 2.5. van Deemter plots (H vs. u) and fitting statistics for uracil, aprotinin, and thyroglobulin obtained under non-retaining conditions.

There are a number of aspects that can be gleaned from the van Deemter characteristics. First, it is clear that the C-CP fiber system is A-term limited, with

this value being independent of the test molecule; as it should be. Clearly, the plate heights seen for uracil reveal that the C-CP fibers are unsuitable for high-resolution, small-molecule separations. Second, because of the experimental condition limitations (flow rates below 0.01 mL min^{-1} (0.5 mm s^{-1}) were unstable with this LC system), the data from the B-term dominated zone were not sufficient to precisely determine the B-terms. Only aprotinin provided a few data points reflecting the B-term dominated zone, so its B-term (0.564 mm^2 s^{-1}) is higher than uracil (0.196 mm^2 s^{-1}) and thyroglobulin (0.190 mm^2 s^{-1}) when fit by MATLAB. Finally, as is clearly shown graphically and in the extracted parameters, the totally-excluded protein (thyroglobulin) shows virtually no C-term contributions to band broadening, with the polypeptide also showing a fair level of immunity to broadening at high-velocity. This result solidly reflects the PSD results presented in former section, and also the previously demonstrated improvements in chromatographic resolution realized with increased linear velocities; up to 100 mm s^{-1} [31]. As a salient point, the differences seen across the molecular sizes call into question the use of uracil as an “un-retained” marker compound in C-CP fiber separations, as clearly it experiences appreciable entropic hold-up within the fiber pores that is not seen for the target protein species.

The near-absence of C-term broadening for thyroglobulin is consistent with other fibrous stationary phases. Ladisch and co-workers [47] generated van Deemter responses for a range of small- and macromolecular polyethyleneglycol (PEG) probes across three different, continuous, fibrous stationary phases; 100%

cotton, cotton:polyester (60:40), and DEAE derivatized cotton/polyester (60:40). Linear velocities of up to 5 mm s^{-1} were evaluated. In each of the phases, the 200 Da PEG probe showed slightly higher plate heights, with some level of C-term broadening, while probes of >20,000 Da showed no broadening as a function of linear velocity. As would be expected, the plate heights derived for the macromolecules varied as a function of the physical structure of the yarn-filled columns (fill, warp, and bias directions) as well as the fiber identity, with the lowest reported values for each being 12 mm for 100% cotton, 8 mm for the cotton:polyester blend, and 2 mm for the DEAE-derivatized material. The 6 mm H-values seen for the C-CP fiber columns seem quite reasonable in light of the base fiber structures.

Besides the verification of pore structure, the very low C term value of thyroglobulin (2 ms) also reflects the fast solute mass transfer of proteins on the C-CP fiber phase. As the C term in van Deemter equation represents the mass transport to and from the bulk mobile phase and sorption and desorption of the solute from the stationary phase, the very low C term suggests the solute reaches the fiber surface by convection but not by diffusion; significantly accelerating the separation. The unique structure of parallel channels set up in the C-CP fiber column, yields exceedingly high levels of shear (>20,000 s^{-1}) which lead to enhanced mass transport by the thinning of diffusion layers (δ) [48,49]. Beyond this, Péclet numbers (Pe) numbers for C-CP protein separations of $>10^6$ clearly point to convective transport occurring at far greater rates than diffusional transport.

Siouffi has presented a comprehensive evaluation of van Deemter C-terms reported for silica- and polymer based monolith columns [50], where mass transfer limitations are controlled by the mesopore structure of the phases. Unfortunately, that review does not include solutes of >6000 Da. In the case of silica monoliths, the highest molecular weight probe was insulin (5807 Da) which yielded at C-term of 10.3 ms, and for polymeric monoliths bradykinin (1060 Da) was reported to yield a C-term of ~12 ms. Other than a few cases involving small molecule separations in capillary formats, these PP C-CP fibers demonstrate superior immunity to mass transfer limitations (lower C-terms). This is particularly important in terms of process applications given the exceptionally high linear velocities employed in the present system.

Implications of the PSD as manifest in Knox plots

The chromatographic behavior of small molecules (organic or inorganic solutes) and large molecules (proteins) on the same chromatographic column are usually quite different. These differences are due to the physical structures of the phases [51]. Thus criteria to evaluate and compare column performance must include the packing material size and solute diffusive properties. The Knox equation [52] with reduced linear velocity and reduced plate height serves to normalize separation quality as a function of the particle diameter:

$$h = Av^{1/3} + B/v + Cv \qquad \text{Eq. 2.8}$$

where *h* is reduced plate height equals to H/d_p where H is common plate height and d_p is the size of packing material (more specifically the equivalent particle or "characteristic" diameter). *v* is the reduced linear velocity ($v = ud_p/D_m$), where u is bulk linear velocity and D_m is solute diffusion coefficient. D_m ($cm^2\ s^{-1}$) can be calculated for modest-sized molecules through the Wilke-Chang equation [53]:

$$D_m = 7.4 \times 10^{-8} \frac{(\psi_B M_B)^{0.5} T}{\eta {V_A}^{0.6}} \qquad \text{Eq. 2.9}$$

where V_A is solute molecular volume, T is temperature, η is mobile phase viscosity, M_B is molecular weight of the solvent, $\psi_B$is association factor. The D_m values of aprotinin and uracil were calculated as 5.42×10^{-7} $cm^2\ s^{-1}$ and 9.82×10^{-6} $cm^2\ s^{-1}$ (with T = 293 K, ψ_B=2.5 [53], and η=1.57 cP [54]). Equation 2.9 is prone to greater errors for high molecular weight solutes, such as proteins. In the case of thyroglobulin here, the formulation presented by Young et al. [55]:

$$D_m = 8.34 \times 10^{-8} \frac{T}{\eta M^{1/3}} \qquad \text{Eq. 2.10}$$

was employed. Using the same experimental conditions as above, the diffusion coefficient of thyroglobulin was computed to be 1.78×10^{-7} $cm^2\ s^{-1}$.

In C-CP fiber columns, where there is no explicit particle diameter to refer to, so fitting to the Knox equation is problematic. Ladisch and co-workers chose to use the width of the fabric yarns (individual fibers twisted together) to set the d_p value [39,56], treating each yarn as a single entity. Different from the yarns in those works, it is believed that the C-CP fibers act somewhat independently in

terms of setting flow characteristics. Therefore, initial fitting to the Knox equation employed the fiber diameter as the particle size (d_p= 37 µm) is shown in Fig. 2.6a along with a tabulation of the statistics.

a.

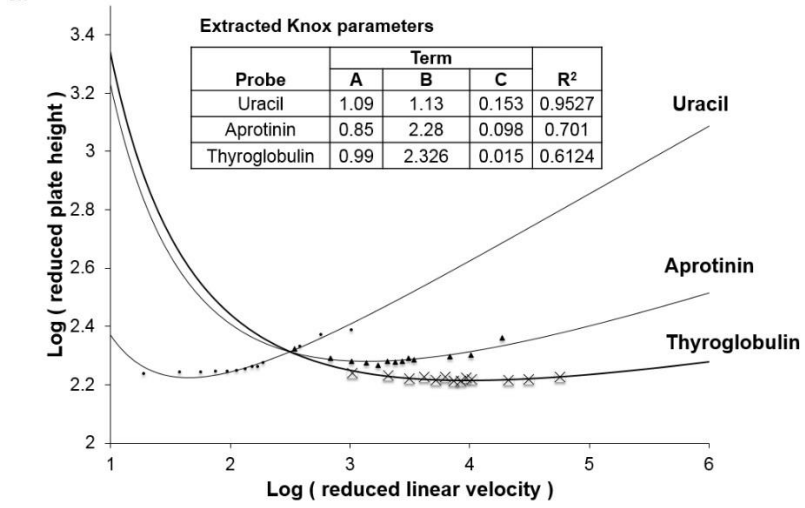

b.

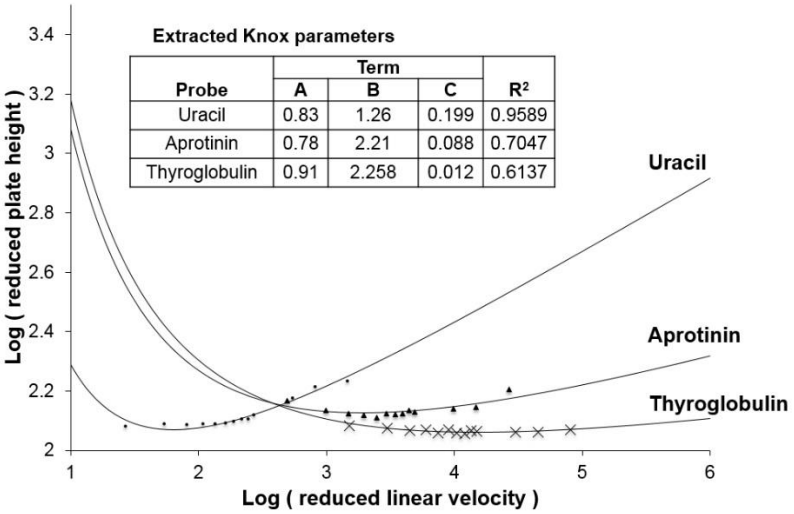

Fig. 2.6. Knox plots (log *h* vs. log *v*) and fitting statistics for uracil, aprotinin, and thyroglobulin obtained under non-retaining conditions based on characteristic diameters (d_p) corresponding to a) the fiber diameter of 37 µm, and b) best-fit diameter of 53 µm.

Very striking is the fact that the highest efficiency protein separations occur at reduced linear velocities that are two orders of magnitude greater than optimum for small molecules (uracil). As tabulated, thyroglobulin has the smallest C-term, uracil has the largest C-term and aprotinin is in between them. While the graphic fits do not look different among the probes, the statistics reveal that the goodness-of-fit (R^2) deteriorates with the increased molecular weights. This is to be expected as the C-terms become virtually non-existent for the peptide and the protein.

In order to determine the validity of the choice of using the fiber diameter as "d_p" to calculate *h* and *v*, the chromatographic data were fit to a range of particle diameters to elucidate the characteristic diameter which best describes the behavior for uracil, aprotonin, and thyroglobulin. The adjusted R^2 values achieved from different diameters derived by MATLAB using a non-linear least squares method and a 95% confidence criteria are presented in Fig. 2.7. Characteristic diameters ranging from 5 – 100 µm were initially input in 5 µm increments, with 1 µm increments used in the size range of greatest correlation. The ability of the Knox equation to be a good descriptor of the system is vastly diminished for the peptide and the protein. The general shapes of the responses (most easily seen for uracil and aprotinin) show better fits with increasing d_p, leveling to an appreciable extent above 40 µm, with the highest adjusted R^2 values appearing at 53 µm and 52 µm in uracil and aprotinin, respectively. The fits improve mildly for thyroglobulin with increasing diameter. From the basic Knox equation, very small C-terms will give way to the velocity dependence in the A-term ($Av^{1/3}$) that *h* will

keep increasing beyond the region dominated by the B-term. To the extreme, thyroglobulin, being a fully-excluded probe, has virtually no C-term as desired by the Knox equation, and often results in negative coefficients and so its adjusted R^2 values are low (~0.55) across the board.

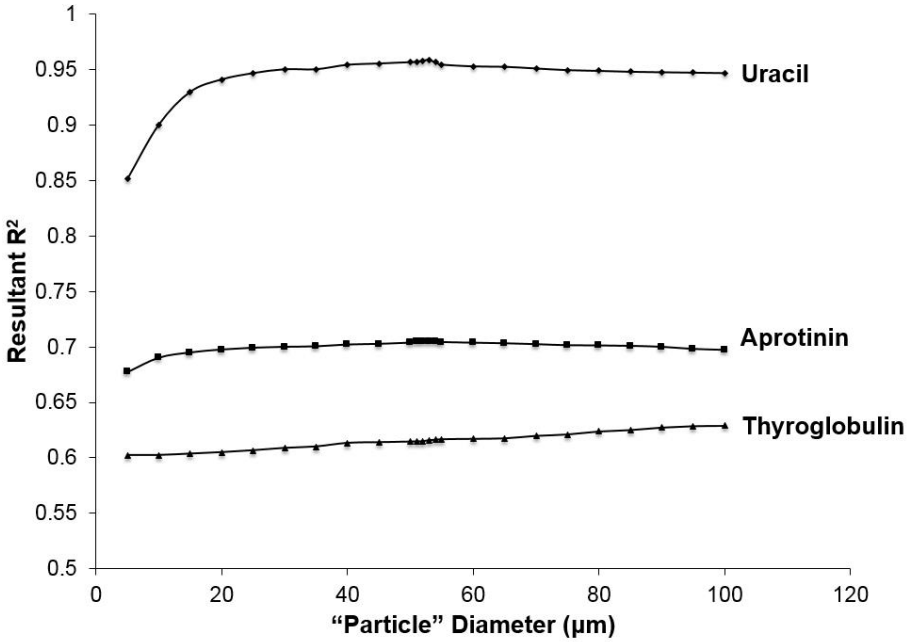

Fig. 2.7. Correlation coefficients determined for fitting of uracil, aprotinin, and thyroglobulin behavior to the Knox equation as a function of characteristic diameters (d_p).

Based on the best-fit correlations for uracil and aprotinin, the most logical characteristic diameter for the PP fiber column is 53 µm. Using this value in computing the *h* and *v* values for the three probe species, the Knox fits are presented in Fig. 2.6b along with the fitting statistics. As suggested by the responses in Fig. 2.7, there is little difference between the fits for the 37 and 53 µm characteristic diameters. One difference, though are the actual *h* and *v* values, which are proportionally reduced by using the high d_p values. This points to a problem in using d_p in ill-defined (non-particulate) systems, as the efficiency

improves, de facto, by choosing large characteristic diameters. In comparison to the other fiber stationary phases, PP fiber has higher reduced plate heights ($10^{2.08} \approx 120$) than the synthetic fibers Nomex and Kevlar fiber (>50) and the cotton-based yarns (~10-30) measured by PEG 20,000 [39,56]. The differences here lie simply in the fact that the other fiber works chose to use yarn widths instead of individual fiber diameters ((200 - 275 μm vs 13 – 20 μm) as the characteristic diameter.

Conclusion

Previous reports of the use of C-CP fiber phases for the separation of proteins demonstrated the unique characteristics of improved chromatographic efficiency and processing figures of merit at elevated linear velocities. By the same token, appreciable broadening was noted for small molecules as linear velocity was increased. These basic characteristics reflect very efficient mass transfer, with minimal hold-up, of macromolecules; i.e. limited porosity on the size scale accessible to proteins. The pore size distribution (PSD) for polypropylene C-CP fibers was determined across a broad range of probe species via inverse size exclusion chromatography (iSEC). Based on the elution characteristics (under non-retaining conditions), an average pore diameter of 4.2 ± 1.1 nm was derived based on the assumption of a Gaussian PSD. Processing of the retention data in a log-nomal mode yielded values of 4.0 ± 0.1 nm. The similarity of the values lends support for the overall PSD characterization. Based on these values, the C-CP fibers are essentially non-porous with respect to large polypeptides and proteins.

While a lack of porosity, and by extension specific surface area, is detrimental towards equilibrium binding capacities, it bodes well in terms of the ability to operate at high linear velocities without mass transfer-imposed penalties. The freedom from such limitations was revealed in both van Deemter and Knox plots generated for uracil, aprotinin, and thyroglobulin at linear velocities of up to 27 mm s^{-1}. Uracil, and to a lesser extent aprotinin, does experience hold-up in the polymer pore structure, but indeed the protein showed no C-term contributions to broadening. In every case, though, column efficiency is limited by A-term factors. While this overall situation is very problematic in isocratic small molecule separations, the ability to perform protein separations (which occur under gradient conditions) at high linear velocities yields many practical benefits in terms of resolution, throughput, and yield [31,33,57].

The high permeability of C-CP fiber columns allows one to capitalize on the efficient mass transfer characteristics found for protein separations. Future studies will build upon these basic characterization studies to better map out the operational space of C-CP fiber columns in terms of both analytical and preparative separations. For example, use of high linear velocities and slow gradients should affect very high peak capacities as needed for analytical protein separations prior to mass spectrometry detection. As a complement, high linear velocities provide dynamic binding capacities that are not appreciably lower than equilibrium-based values, thus making them cost- and time-efficient in preparative situations. Finally, the favorable physical aspects of protein separations of C-CP fiber phases will be

extended to systems having greater chemical selectivity though the use of diverse polymer surface modification strategies.

References

[1] U.D. Neue, HPLC Columns Theory, Technology, and Practice, Wiley-VCH, New York, 1997.

[2] R.L. Cunico, K.M. Gooding, T. Wehr, Basic HPLC and CE of Biomolecules, Bay Bioanalytical Laboratory, Richmond, CA, 1998.

[3] M. Leonard, J. Chromatogr. B, 699 (1997) 3.

[4] M. Ousalem, X. Zhu, J. Hradil, J. Chromatogr. A, 903 (2000) 13.

[5] Y. Yao, A. Lenhoff, J. Chromatogr. A, 1037 (2004) 273.

[6] H.L. Ritter, L.C. Drake, Ind. Eng. Chem. Anal. Ed., 17 (1945) 782.

[7] R.W. Cranston, F.A. Inkley, Adv. Catal., 9 (1957) 143

[8] N. Pernodet, M. Maaloum, B. Tinland, Electrophoresis, 18 (1997) 55.

[9] M. Baklanov, K. Mogilnikov, V. Polovinkin, F. Dultsev, J. Vac. Sci. Technol. B, 18 (2000) 1385.

[10] M. Al-Bokari, D. Cherrak, G. Guiochon, J. Chromatogr. A, 975 (2002) 275.

[11] H. Guan, G. Guiochon, J. Chromatogr. A, 731 (1996) 27.

[12] D. Lubda, W. Lindner, M. Quaglia, C. von Hohenesche, K. Unger, J. Chromatogr. A, 1083 (2005) 14.

[13] H. Barth, B. Boyes, C. Jackson, Anal. Chem., 70 (1998) 251R.

[14] Aggebran.L, Samuelso.O, J. Appl. Polym. Sci., 9 (1965) 639.

[15] J. Knox, H. Scott, J. Chromatogr., 316 (1984) 311.

[16] K. Jerabek, K. Setinek, J. Hradil, F. Svec, React. Polym., 5 (1987) 151.

[17] A. Gorbunov, L. Solovyova, V. Pasechnik, J. Chromatogr., 448 (1988) 307.

[18] J. Giddings, E. Kucera, C. Russell, M. Myers, J. Phys. Chem., 72 (1968) 4397.

[19] B.A. Grimes, R. Skudas, K.K. Unger, D. Lubda, J. Chromatogr. A, 1144 (2007) 14.

[20] J. Stahlberg, B. Jonsson, C. Horvath, Anal. Chem., 63 (1991) 1867.

[21] P. DePhillips, A. Lenhoff, J. Chromatogr. A, 883 (2000) 39.

[22] Y. Rouault, S. Assouline, Powder Technol., 96 (1998) 33.

[23] D. Moravcov, P. Jandera, J. Urban, J. Planeta, 26 (2003) 1005.

[24] Y. Li, H.D. Tolley, M.L. Lee, J. Chromatogr. A, 1217 (2010) 8181.

[25] P. DePhillips, A. Lenhoff, J. Chromatogr. A, 883 (2000) 39.

[26] R.K. Marcus, W.C. Davis, B.C. Knippel, L. LaMotte, T.A. Hill, D. Perahia, J.D. Jenkins, J. Chromatogr. A, 986 (2003) 17.

[27] R.D. Stanelle, R.K. Marcus, Anal. Bioanal. Chem., 393 (2009) 273.

[28] A.J. Schadock-Hewitt, J.J. Pittman, K.A. Stevens, R.K. Marcus, J. Appl. Polym. Sci., 128 (2013) 1257

[29] R.D. Stanelle, L.C. Sander, R.K. Marcus, J. Chromatogr. A, 1100 (2005) 68.

[30] K.M. Randunu, S. Dimartino, R.K. Marcus, J. Sep. Sci., 35 (2012) 3270.

[31] K.M. Randunu, R.K. Marcus, Anal. Bioanal. Chem., 404 (2012) 721.

[32] D.M. Nelson, R.K. Marcus, Protein Peptide Lett., 13 (2006) 95.

[33] K.M. Randunu, R.K. Marcus, Biotechnol. Prog., 29 (2013) 1222.

[34] Y. Yao, A. Lenhoff, J. Chromatogr. A, 1037 (2004) 273.

[35] C.Q. Burdette, R.K. Marcus, Analyst, 138 (2013) 1098.

[36] E.R. Nightingale, J. Phys. Chem., 63 (1959) 1381.

[37] K. Nishida, Y. Ando, H. Kawamura, in, Colloid. Polym. Sci., 261 (1983) 70.

[38] M. Brissová, M. Petro, I. Lacík, A.C. Powers, T. Wang, Anal. Biochem., 242 (1996) 104.

[39] K. Hamaker, J.Y. Liu, C.M. Ladisch, Biotechnol. Prog. 14 (1998) 21.

[40] A.E. Rodrigues, V.G. Mata, M. Zabka, L. Pais, in F. Svec, T.B. Tennikova, Z. Deyl (Editors), Monolithic Materials: Preparation, Properties, and Applications, Elsevier Science, BV, Amsterdam, 2003.

[41] P. Jandera, M. Stankova, V. Skerikova, J. Urban, J. Chromatogr. A, 1274 (2013) 97.

[42] Y. Yao, A.M. Lenhoff, J. Chromatogr. A, 1126 (2006) 107.

[43] H. Oberacher, A. Premstaller, C.G. Huber, J. Chromatogr. A, 1030 (2004) 201.

[44] J.M. Randunu, S. Dimartino, R.K. Marcus, J. Sep. Sci., 35 (2012) 3270.

[45] J.H. Knox, H.P. Scott, J. Chromatogr A, 282 (1983) 297.

[46] D.K. Nelson, R.K. Marcus, Anal. Chem. 78 (2006) 8462.

[47] K. Hamaker, J.Y. Liu, C.M. Ladisch, Biotechnol. Progress, 14 (1998) 21.

[48] M. Leveque, Ann. Mines., 13 (1928) 284.

[49] C.F. Wertz, M.M. Santore, Langmuir, 18 (2002) 1190.

[50] A.M. Siouffi, J. Chromatogr. A, 1126 (2006) 86.

[51] L.R. Snyder, M. Stadalius, M.A. Quarry, Anal. Chem., 55 (1983) 1412A.

[52] J.H. Knox, J. Chromatogr. A, 15 (1977) 352.

[53] C. Wilke, P. Chang, AIChE Journal, 1 (1955) 264.

[54] L.R. Snyder, J.J. Kirkland, J.W. Dolan, Introduction to Modern Liquid Chromatography, Wiley.

[55] M. Young, R. Carroad, R. Bell, Biotechnol. Bioeng. 22 (1980) 947.

[56] Y. Yang, A. Velayudhan, C.M. Ladisch, M.R. Ladisch, J. Chromatogr. A, 598 (1992) 169.

[57] D.M. Nelson, R.K. Marcus, Protein Peptide Lett. 13 (2006) 95.

CHAPTER THREE

ROLE OF INTERSTITIAL FRACTION AND LOAD VELOCITY ON THE DYNAMIC BINDING CAPACITY OF PROTEINS ON CAPILLARY-CHANNELED POLYMER (C-CP) FIBERS COLUMNS

Introduction

Since the first description of liquid chromatography (LC) separations of proteins via ion exchange on cellulosic supports [1], the evolution of stationary phases used for protein analytics and downstream processing applications is a story of the contrarian aspects of thermodynamics and kinetics. Early polysaccharide-based stationary phases, such as cross-linked dextran [2], showed advantages in low materials costs and relative immunity to on-column protein denaturation. However, poor physical robustness due to the 'softness' of the material restricts the use of high linear velocity/high operating backpressures in processing [3]. The introduction of 'harder' stationary phases such as modified silica [4], opened up the potential for higher mobile phase velocities and larger bed volumes, while providing higher equilibrium binding capacities due to their porosity and corresponding higher specific surface areas. In the realm of small molecule LC, particle diameters of <2 μm and porosities of >80% provide for incredibly high separation efficiencies with plate heights of 2 μm [5]. These thermodynamic-based advantages are lost in the separation of macromolecules such as proteins and oligonucleotides as the kinetics of through-pore diffusion greatly restrict the

practical separations speeds. In the extreme, the high intra-pore surface areas are wasted as they are not accessed by species of large hydrodynamic radii.

In an effort to overcome the kinetic (i.e., mass transfer) limitations of small diameter, high porosity phases, non-porous [6,7]or superficially porous [8-10] particles having larger diameters have been the focus of a great deal of effort in terms of analytical and preparative protein separations. Decreasing particle diameters increase the binding capacity to a certain degree, but the accompanying high backpressures come with operational overhead challenges. Greater interest lies in the use of in this regard, column throughput is gained via higher mass transfer rates, at the expense of lower binding capacity, due to the lower overall lower porosity.

Stationary phases which address compromises among the factors of chemical flexibility, mass transfer, binding capacity, physical robustness, and stability in various mobile phases are needed to increase the efficiency of macromolecule separations, particularly as they apply to downstream processing applications [11,12]. To this end, monolithic stationary phases, synthesized from both inorganic (silica-based) or polymeric materials, are an attractive option [13-15]. The ability to affect high fluidic transport efficiencies (in bulk), with very short diffusion distances within the mesoporous structure addresses some of the kinetic limitations of particulate phases [16]. Likewise, the diversity of chemical formats provides a rich palette from which various separation modalities can be affected. Indeed, very high separation efficiencies and speeds have been realized on the

analytical scale using monolithic stationary phases. Unfortunately, the practical realization of monolithic preparative-scale assemblies continues to be a challenge.

Beyond particle and monolith phase formats, there continues to be extensive effort placed toward the development alternative phases and approaches [17-19]. As stated above, in each case, there is a continual interplay between the thermodynamic/ equilibrium and kinetic aspects in how each phase might be employed in either analytical or preparative (i.e., downstream processing) applications. To this end, fibrous stationary phases have been the topic of some interest for approximately 30 years [20-25]. As reviewed by Marcus [26,27], fibrous phases have a number of physical, chemical, and economic attributes that suggest their use, particularly in preparative situations. Perhaps the most substantive early works in this area were those of Ladisch and co-workers, who demonstrated the utility of textile fabrics to affect protein separation in a variety of chromatographic modes [21,23,28,29]. Those works, among other things, demonstrated the ability to affect high fluidic flow rates, without severe backpressure or solute mass transfer penalties. The key aspects here are a highly porous bed, with short inter-fiber diffusion distances, and a lack of intra-fiber porosity. In chromatograph terms, the efficiencies are dominated by aspects of the van Deemter A-term (i.e., bed homogeneity), with a virtual absence of C-term broadening [21,23]. Subsequent work by Pinto and co-workers [24,30] illustrated the chemical diversity that could be affected based on the choice of base fiber composition. For example, polysulfone microfibers could be randomly-packed in traditional column structures

to affect ion exchange separations of proteins. In this case, the fibers had appreciable porosity, such that slow intra-fiber diffusion limited the hydrodynamic ability to operate at high solvent flow rates.

Capillary-channeled polymer (C-CP) fibers are being developed in this laboratory as stationary phases for protein separations in ion-exchange (IEC), reversed phase (RP), and hydrophobic interaction (HIC) chromatography modes [31-33]C-CP fibers are melt-extruded from commodity polymers (polypropylene, polyester, and nylon 6), such that eight channels are formed along the fiber axis. The fibers are continuously extruded to lengths of many kilometers, with nominal diameters of 30 - 60 µm, with channel diameters ranging from 5 – 25 µm. When C-CP fibers are packed into column structures, the channel walls (legs) of adjacent fibers interdigitate, to effectively form capillary channels of 1 – 5 µm width which run parallel down the length of the column. A high porosity structure results, allowing for high solvent flow rates at low backpressures. Recent studies have shown that the C-CP fibers are virtually non-porous on the size scale of proteins (with average pore diameters of ~4 nm) [34], thus there is no intra-fiber diffusion. As a cumulative result, C-CP fiber columns can be employed for analytical scale protein separations at extremely high linear velocities ($U_o \approx 100$ mm s^{-1}), and low backpressures (<2000 psi) [35,36]. On the other hand, small molecule separations are more favorable performed a low linear velocities. Interestingly, for small molecules, there is a trade-off between achieving longer retention times at high fiber packing densities (low interstitial fractions) and more narrow peaks at higher

interstitial fractions [35]. So, there is a contradiction between thermodynamic and kinetic effects. The favorable hydrodynamic qualities for protein separations par well with the diversity of chemistries presented by the different base polymers as well as a broad palette for surface modifications to affect the chemical selectivity of separations.

This group recently reported the practical characteristics of C-CP fiber columns in terms of the throughput and yield for the ion exchange processing of aqueous solutions of the protein lysozyme [37]. As might be expected, the ease of fluidic flow, short inter-fiber diffusion distances, and lack of fiber porosity act in concert to provide very high processing efficiencies for the analytical-scale columns, with a throughput of 0.2 mg min^{-1} processed on a column containing only 78 mg of fiber at a fairly low lysozyme concentration of 0.2 mg mL^{-1}. As described above, the analytical chromatographic efficiencies for proteins on C-CP fiber columns have been evaluated in terms of column packing parameters (interstitial fraction/packing density) and solution linear velocities, but these relationships have not been established with regards to downstream protein processing.

We describe here results of studies first assessing the equilibrium binding capacity (EBC) of C-CP fibers for bovine serum albumin (BSA) on nylon 6 C-CP fibers and then determining the dynamic loading characteristics as a function of the column interstitial fraction (packing density) and mobile phase linear velocity using frontal analysis (FA) as the quantitative methodology. The chemical functionality of nylon 6, amide moieties within short alkyl chains, provide a fairly

hydrophilic surface, with the presence of ionized end groups making it a good surface to affect ion exchange separations. Adsorption isotherms are evaluated for both static and dynamic cases using Langmuir, Freundlich, and Moreau models. As in the previous evaluation of chromatographic efficiencies, trade-offs between the fiber surface area available for adsorption (i.e., fiber packing density) and the ready access to that surface area are seen. The rapid mobile phase-surface transport kinetics of the proteins permit high capture efficiencies (relative to static conditions) at linear velocities of up to 12.5 mm s^{-1}. These studies provide a basis for the scale-up of C-CP fiber columns, looking towards applications in downstream processing of proteins for a variety of end applications.

Materials and Methods

Reagents and Chemicals

Bovine serum albumin (BSA) from Sigma-Aldrich (Milwaukee, WI), hydrochloric acid (HCl) from J.T. Baker (Center Valley, PA), TRIS-HCl buffer (1M, pH 8.0) from Teknova (Hollister, CA), and Milli-Q water (18.2 MΩ cm^{-1}) were used to prepare analyte solution. HPLC grade acetonitrile (ACN) from Millipore (Billerica, MA) and HPLC grade methanol from Alfa Aesar Ward (Hill, MA) were employed to wash the column. Uracil and glucose oxidase both from Sigma-Aldrich (Milwaukee, WI) were utilized to measure the interstitial fractions of columns.

BSA was chosen as analyte in this experiment because of its ubiquitous use across analogous studies of other phases and previous works from this

laboratory [38,39]. The test solution was prepared by mixing BSA into Milli-Q water at a concentration of 1 mg mL^{-1}. The pH was adjusted using HCl to a value of 7.0, with the pH was buffered by 20 mM TRIS. It is important to note that, in a pH = 7 environment, the polymer end groups of nylon 6 are zwitterionic, having both negative and positive charges. Based on the isolelectric point of BSA, pI = 4.7, the protein has a net negative charge, and so the interaction with the fiber surface is a combination of electrostatic (i.e., the cationic fiber sites), hydrogen bonding, and hydrophobic interactions.

C-CP Fiber Column Preparation

As in previous works, the nylon 6 C-CP fibers employed in this study were extruded in the School of Materials Science and Engineering of Clemson University [40]. These specific fibers were extruded as 30-filament yarns, with each filament having a nominal diameter of ~25 µm and a measured perimeter of 207.5 µm. The column assembly protocol has been described in detail [25]. Columns were prepared here by pulling fibers through 4.6 mm inner diameter (i.d.), 25 cm stainless steel tubing (from Grace Davison Discovery Sciences, Deerfield, IL). In order to achieve a range of column interstitial fractions, and thus stationary phase masses, columns were prepared by pulling 15,600, 17,400, 19,200, 21,000, and 22,800 fibers through the columns. Once assembled, the fiber columns were washed with ACN, methanol, and Milli-Q water in sequence in order to remove the residual anti-static detergent coatings [31]. The interstitial fractions were determined for each column using both uracil and glucose oxidase as probe

species, injected under non-retaining conditions. C-CP fiber columns require no specific storage conditions, with the columns sealed with traditional fittings with aqueous solutions in the tubing. Table 3.1 provides a summary of the physical characteristics of the 5 columns employed in these studies.

Table 3.1. Physical characteristics of the nylon 6 C-CP fiber columns employed in these studies.

Number of fibers	Fiber mass (g)	Interstitial fraction (ε_i)	Total fiber surface area (m^2)
15,600	1.56	0.546	8.09
17,400	1.73	0.523	9.03
19,200	1.91	0.508	9.96
21,000	2.10	0.460	10.9
22,800	2.29	0.401	11.8

Chromatographic System and Operations

The chromatographic system consisted of a Dionex (Sunnyvale, CA) Ultimate 3000 unit composed of a LPG-3400SD pump, a WPS-3000TSL autosampler, and a VWD-3400 RS UV-Vis absorbance detector. C-CP fiber columns were simply mounted in the same position as standard packed bead columns. The Dionex Chromeleon software (Sunnyvale, CA) and the Microsoft Excel (Seattle WA) were utilized to collect and process the data respectively. Protein concentration determinations made in discrete solutions were performed in a NanoVue Plus spectrophotometer from (GE Healthcare, Pittsburgh, PA) at a measurement wavelength of 216 nm (amide absorption maximum), with calibration curves prepared in the working buffer system.

Fiber Loading Studies

The adsorption characteristics of a particular sorbent provide important information about the thermodynamic and kinetic properties of that material [41,42]. In the realm of preparative chromatography, the two operational regimes of interests are the equilibrium (i.e., steady state or static) and dynamic binding capacities. The equilibrium binding capacity (EBC) is extracted from data determined by stirring or shaking a container which contains the adsorbate proteins in a representative solvent and a known amount of unpacked stationary phase and allowing to the phases to come to equilibrium (usually over a period of hours) based on solute diffusion to the sorbent surface [43]. The difference in protein concentration in the solvent before and after the exposure time is a reflection of the amount of material that has adsorbed onto the stationary phase. Microsamplings of the solvent composition as a function of time serve as an indicator of the sorption kinetics and mechanisms, and to confirm the attainment of a steady state. In the simplest case, the amount adsorbed reflects the number of *active sites* on the phase, though as will be described in subsequent sections many physico-chemical non-idealities can occur. In this work, 50 mL volumes of a range of BSA concentrations in 20 mM TRIS were exposed to 1.56 g of nylon 6 C-CP fiber (equating to the lowest density packed columns) in 100 mL beakers with magnetic stir bars. The initial evaluation of the protein uptake (performed at a BSA concentration of 1.0 mg mL^{-1}) involved taking 2 µL aliquots for absorbance determinations at intervals starting at 20 min for the 5 hours, and then hourly for a

total of 24 hours. That study indicated that the vast majority of adsorption occurred over the first 6 hours, but for the sake of completeness, subsequent studies were performed for a 24 hour exposure, under constant stirring.

In contrast, adsorption data used to determine the dynamic binding capacity (DBC) is derived by measurements performed in a packed column under flow conditions. The amount of protein binding to the column under a given set of experimental conditions is determined through the generation of breakthrough curves [41]. Frontal analysis (FA) is a versatile method to evaluate dynamic absorption data (via breakthrough curves) to determine kinetic and thermodynamic properties of a given packing material [44,45]. While the accuracy of FA is dependent on the control of several experimental factors such as temperature, column pressure, and mobile phase composition, and the accurate determination of column dimensions and interstitial fraction [46], its primary advantages are its mathematical and experimental simplicity. The method's independence of the column's chromatographic efficiency and the solute mass transfer kinetics make it particularly attractive in the case of C-CP fiber columns which present several-millimeter plate heights in small molecule separations [35,47].

The theoretical and practical basis for the FA employed here was described by Vera-Avila and co-workers [48], and implemented exactly as in this laboratory's previous work. For each of the loading capacities reported here, the experiments were run as triplicates with the adsorbed protein removed from the fibers with a flow of 100% ACN to such point as the absorbance measured post-column was

returned to a stable baseline value. This wash step was performed at a volume flow rate of 1 mL min^{-1}, with a typical exposure time of 20 – 30 min. As evidence of the utility of the wash procedure, the loading capacity of the individual C-CP fiber columns did not change across the entirety of the experimental matrix.

Results and Discussion

Equilibrium binding capacity (EBC)

Implicit in the discussion above, the EBC represents the total amount of protein adsorbed onto the substrate over the total period of the exposure, without regards to the actual mechanism of adsorption. The performance of adsorption experiments across a range of solute concentrations allows for the extraction of mechanistic information as well as setting relevant parameters for practical protein isolation procedures. Adsorption isotherms can be constructed from either static or dynamic loading experiments, with the fits to different models depicting the forms of the liquid-solid equilibrium for that solute as well as predicting the loading capacity for the adsorbate-adsorbent pair. The experimental conditions of batch equilibrium studies were as described above, performed for BSA concentrations ranging from 0.1 – 1.2 mg mL^{-1} in 20 mM TRIS. Triplicate 50 mL test volumes were placed in 100 mL beakers in the presence of 1.56 g of nylon 6 C-CP fibers and stirred for a period of 24 hours. The amount of adsorbed proteins was determined by difference in the absorbance of the test solution before and after exposure.

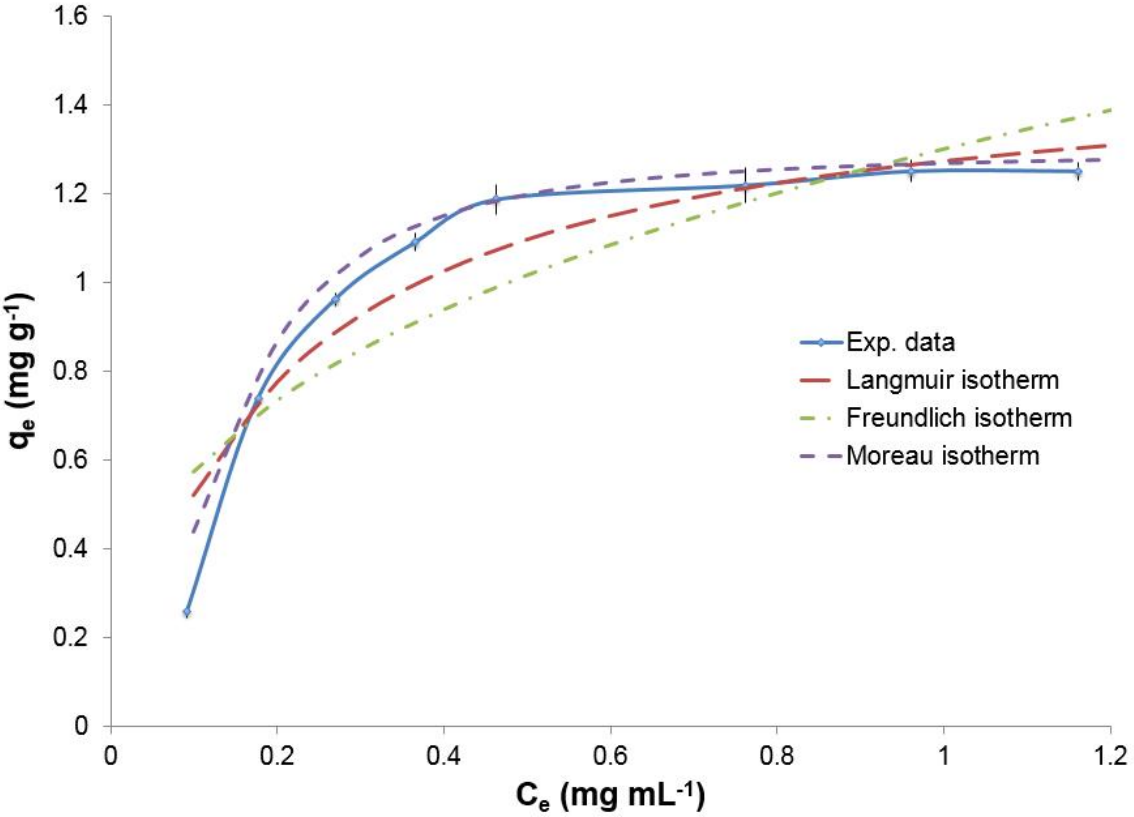

Fig. 3.1. Experimental data and regression fits for different isotherm models for the determination of the equilibrium binding capacity (EBC) of BSA on nylon 6 C-CP fibers. Initial BSA concentrations = 0.1 - 1.2 mg mL^{-1} in 20 mM TRIS, exposure time = 24 hours.

Figure 3.1 presents the results of the EBC studies in the form of an adsorption isotherm; the determined adsorbed mass per unit mass of support (q_e, mg g^{-1}) versus the exposed solute concentration (C_e, mg mL^{-1}). Clearly seen, the amount of protein adsorbed increases with the solution concentration from 0.1 – 0.4 mg mL^{-1}, but beyond this point increases in protein concentration do not change the amount that could be adsorbed in the 24-hour test period. The physical data was treated here using three common isotherm models which have general relevance in different interaction regimes [49]: the Langmuir isotherm

(adsorbate-adsorbent interactions at a chemically homogeneous surface leading to the formation of a monolayer of coverage), the Freundlich isotherm (adsorbate-adsorbent interactions at a heterogeneous surface leading to the formation of a monolayer of coverage), and the Moreau isotherm (adsorbate-adsorbate interactions following the establishment of a monolayer of coverage).

The Langmuir isotherm [41,50]has been widely used to present many real adsorption processes and is expressed as:

$$q_e = \frac{q_s b C_e}{1 + b C_e} \qquad \text{Eq. 3.1}$$

where q_e (mg g^{-1}) is the amount of BSA loaded on nylon-6 stationary phase at an equilibrium condition when the initial BSA concentration is C_e (mg mL^{-1}), q_s (mg g^{-1}) is maximum equilibrium binding capacity (sometimes referred to as Q) for BSA bound per unit weight of nylon 6, and b (mL mg^{-1}) is the Langmuir (adsorption-desorption) constant related to the binding site affinity of the solute. Data of q_e and C_e from Fig. 3.1 were fit to Eq. 3.1 within MATLAB (Natick, MA, USA), resulting in a maximum equilibrium binding capacity of q_s = 1.52 mg g^{-1} and an equilibrium constant of b = 5.18, with a least-squares goodness-of-fit of R^2 = 0.91, as listed in Table 3.2. The sharp increasing of q_e in the range of initial concentrations of BSA (0.1 – 0.5 mg mL^{-1}) yields a rectangular isotherm, indicative of a high affinity of the protein for the fiber surface.

Table 3.2. Derived parameters for different isotherm models under both equilibrium and dynamic conditions.

	Equilibrium	Dynamic	Equilibrium	Dynamic	Equilibrium	Dynamic	Equilibrium	Dynamic
Langmuir	q_s (mg g^{-1})		b (mL mg^{-1})				R^2	
	1.52	2.18	5.18	1.02			0.912	0.997
Freundlich	q_s (mg g^{-1})		n				R^2	
	1.3	1.1	2.8	1.57			0.742	0.988
Moreau	q_s (mg g^{-1})		b (mL mg^{-1})		I		R^2	
	1.3	2.07	0.05	1.05	12430	1.17	0.991	0.996

While the regression statistics for the Langmuir fit of the EBC data suggest reasonable agreement, it is clear graphically, that the fit for that model is not a good one. As a first alternative, the Freundlich isotherm [41,51] was also utilized to fit the adsorption data, which is presented as:

$$q_e = Q_f {C_e}^{1/n} \qquad \text{Eq. 3.2}$$

where Q_f (mL g^{-1}) is the Freundlich coefficient which reflects the equilibrium adsorption capacity, n is the Freundlich exponent which indicates the degree of deviation from a linear isotherm, and thus the variation in the driving forces across the heterogeneous surface sites. Incorporation of the raw adsorption data into Eq. 3.2 via a MATLAB routine yielded a Q_f = 1.30 mL g^{-1} and n = 2.80, with a correlation coefficient of R^2 = 0.74, as reported in Table 3.1. It must be stated that the coefficients in the Freundlich mode have little direct physical meaning, but it is clear (visually and via regression statistics) that the model itself does not represent the

interactions occurring in this system.

As neither the Langmuir nor the Freundlich models (which have as their common aspect the formation of monolayer coverage on the surface) reflects the isotherm character depicted in Fig. 3.1, the potential for multilayering must also be considered. Protein-protein interactions on surfaces are very well known, and will occur if given the opportunity (i.e., time) [52-54]. BSA is well known to multilayer in static systems [55,56]. The most common model employed to describe adsorbate-adsorbate interactions, following the initial establishment of a monolayer, is the Moreau isotherm [41,57] presented as:

$$q_e = q_s \frac{bC_e + Ib^2{C_e}^2}{1 + 2bC_e + Ib^2{C_e}^2} \qquad \text{Eq. 3.3}$$

where q_s (mg g^{-1}) is the phase saturation capacity, b (mL mg^{-1}) is low-concentration equilibrium constant, and I is adsorbate-adsorbate interaction parameter which can be written as:

$$I = exp\left(\frac{\in_{AA}}{RT}\right) \qquad \text{Eq. 3.4}$$

where $\in$ is the interaction energy between layers of adsorbed molecules of A, and T is the absolute temperature. It is important to note that in the case of very weak adsorbate-adsorbate interactions ($I \rightarrow 0$) that the Moreau equation basically breaks down to the Langmuir isotherm equation. Fitting of the adsorption data into Eq. 3.3 in MATLAB results in values of q_s = 1.30 (mg g^{-1}), b = 0.05 (mL mg^{-1}), and I = 12,430 with R^2 = 0.991 were obtained by, as presented in Table 3.2. The R^2

obtained for Moreau isotherm model is higher than both Langmuir isotherm and Freundlich isotherms, with the match being visually clear. Finally, the high value for I strongly confirms the existence of adsorbate-adsorbate interactions (i.e., multilayering phenomena) under equilibrium (static) loading conditions. Based on the degree of fit, particularly at the upper range of concentrations, the Moreau and its EBC value of 1.3 mg BSA g^{-1} nylon 6 C-CP fiber are believed to be the best representative of the system.

Dynamic Binding Capacity (DBC)

Interstitial fraction determinations - The dynamic binding capacity (DBC) of a medium is the result of the combination of the thermodynamic and kinetic aspects of the separation; these aspects are inextricably tied together. The chemical thermodynamics drive the relative affinities of the solutes between the mobile and stationary phases. These driving forces work in concert with the phase ratio for the system (β = mobile phase volume/stationary phase volume) to define the equilibrium binding capacity. Solute transport phenomenal and adsorption / desorption kinetics define the extent of surface coverage in the time frame of a specific separation process. While high specific surface areas are generally advantageous in terms of EBC, these are usually achieved through small-diameter, highly porous phases. As such, the diffusion of biomacromolecule solutes from the bulk fluid flow and through the porous structure is the rate-limiting step. In the world of downstream processing, where throughput and yield are often the key processing metrics, the kinetic aspects of the separation can trump the EBC

aspects of a phase material [11,12,58,59].

In the case of C-CP fiber column separations, the interstitial fraction (ε_i = volume of mobile phase/volume column) of the bed is a key physical parameter, linking the available surface area for solute adsorption and the general hydrodynamic throughput. There is an inverse relationship between the number of fibers within the column structure; low interstitial fractions equate to large numbers of fibers, and consequently greater exposed fiber surface area (noting that proteins do not diffuse into the fiber matrix). Interstitial fraction also affects other aspects of the separation. High interstitial fractions result at lower backpressures at a given volume flow rate, while low interstitial fractions result in shorter separation distances between opposing fiber surfaces, and thus overall shorter diffusion distances. Finally, and most kinetically relevant, low interstitial fractions result in higher mobile phase linear velocities for a given volume flow rate; thus the on-column residence time is reduced. We have recently reported on the effects of C-CP fiber interstitial fractions (i.e., fiber packing density) on the chromatographic performance (i.e., peak heights) for the isocratic separation of small molecules and the gradient separation of a suite of proteins [60]. In both instances, interstitial fractions of $\varepsilon_i \approx 0.63$ yielded the best performance, though there can be no assumption that the same fiber packing density would yield the highest dynamic binding capacity.

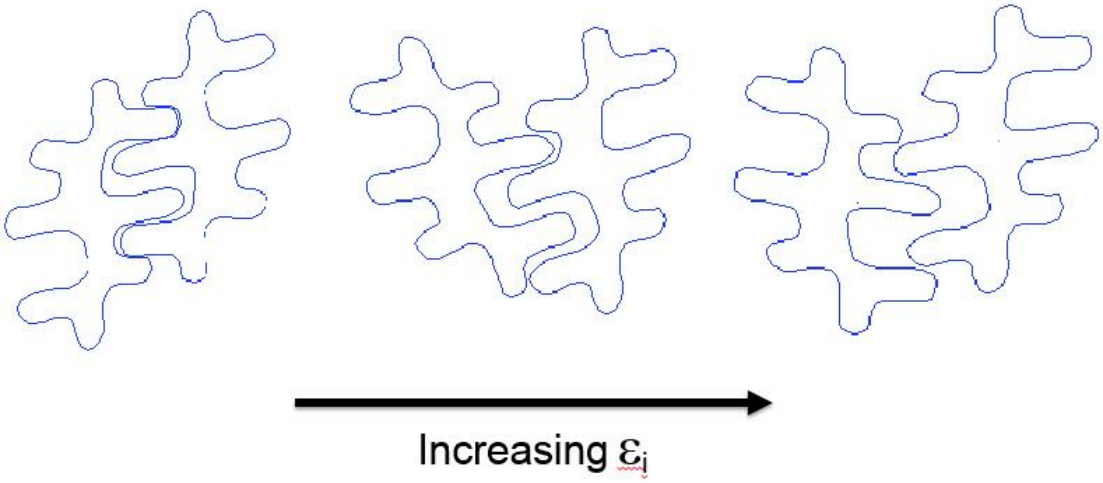

Fig. 3.2. Figurative depiction of the inter-fiber channel structure of C-CP fibers as a function of the column interstitial fraction (ε_i).

In order to understand the role of interstitial fraction on the DBC for C-CP fiber columns, 5 columns having different packing densities were evaluated, ranging from 15,600 – 22,800 fibers (in parallel) per column. While the nucleobase uracil (MW = 112 g mol^{-1}) is the most commonly employed probe molecule for ε_i determinations, previous studies have shown this leads to an overestimation in ε_i as that molecule can access the 4 nm radius pores of the C-CP fibers, while the target proteins solutes are excluded [34]. A more relevant value of the interstitial fraction is obtained using the protein glucose oxidase (MW ≈ 186,000 g mol^{-1}), with both used here to illustrate the differences. (Glucose oxidase was also used as neutral mark in breakthrough curves by deducting its elution times in different columns and flow rates from the curve to achieve the real loading volumes.) Interstitial fractions were determined under non-retaining conditions for the two probe molecules, DI-H_2O for uracil and 90:10 ACN:H_2O for the protein. As shown

in Fig. 3.3 the ε_i values ranged from 0.653-to-0.780 as measured by uracil and 0.401-to-0.546 as measured by glucose oxidase. In both cases, the interstitial fraction values decrease in a fairly linear fashion with increased numbers of nylon 6 C-CP fibers in the columns, with the lower values for the protein reflecting those molecules' lack of access to the fiber pore structure. The fact that the trend lines parallel each other provides support for the general methodology and the intended lack of chemical interactions with the nylon 6 fibers.

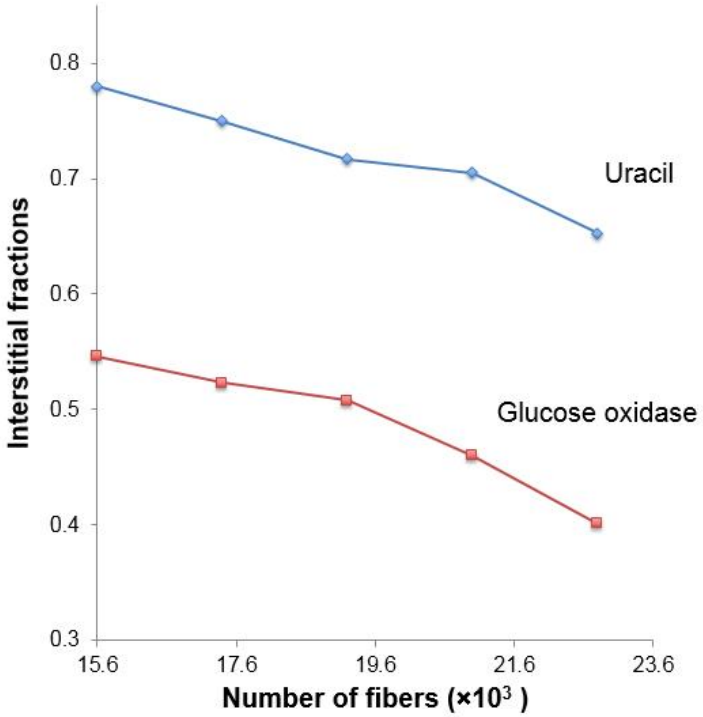

Number of fibers (×10³)	Interstitial fractions	
	Uracil	Glucose oxidase
15.6	0.78	0.546
17.4	0.75	0.523
19.2	0.717	0.508
21	0.705	0.46
22.8	0.653	0.401

Fig. 3.3. Interstitial fractions of C-CP fiber columns employed in these studies as measured by uracil and glucose oxidase probe species.

Role of fiber packing density at fixed volume flow rates – As the nylon 6 fibers are consistently of the same diameter/perimeter, increased numbers of fibers present increased surface area to affect protein adsorption. Table 3.1

presents the total fiber surface area for the five column packing densities. Under conditions of constant volume flow rate, the same molar amount of protein is passed through the column per unit time. Figures 3.4a – e present breakthrough curves for the introduction of BSA at a concentration of 1 mg mL^{-1} in pH = 7.0 aqueous 20 mM TRIS buffer at flow rates of 1 – 5 mL min^{-1}. The individual breakthrough curves are the average of three curves taken under each experimental condition, with the derived values in the accompanying tables being the average of the same.

Inspection of the shapes of the breakthrough curves at a given volume flow rate reflect many of the essential aspects of the adsorption process (with the quantitative figures reported in the tables). Clearly seen is the onset of breakthrough occurs at lower bed volume (BV) values corresponding to fewer numbers of fibers (the $C/C_o = 0.5$ positions are also displaced to lower BV values). This of course reflects the fact that there is less fiber surface area for which BSA can adsorb. Also apparent is the fact that the kinetics of adsorption for the low-density packings are slower than for the high densities. This is seen in two aspects of the breakthrough curves; lower slopes in the transitional region of each curve and much slower approaches to saturation at the top end of the curves. The non-idealities as saturation is being approached are far more prevalent at the highest volume flow rates; as might be expected. The kinetic differences seen in each figure are dictated by the intrafiber separation distances, which decrease as the packing density increases. As such, the short diffusion distances result in transient

responses that are more like step functions.

Quantitatively, the tabulated data are consistent across each volume flow rate. As would be anticipated, the mass of BSA adsorbed at each flow rate increases with the number of fibers per column. Noteworthy, though, is the fact that the mass adsorbed at saturation is not directly proportional to the number of fibers (and thus surface area). For example, the loading capacity value increases by ~27% for the 1 mL min^{-1} experiments, while the actual fiber surface area increases by 46%. Indeed, on a per unit mass basis, the dynamic loading capacity (q_e) decreases from 1.16 – to – 1.00 mg BSA per g nylon 6 C-CP fiber. Clearly, under these sets of conditions, the additional sorbent phase is not fully utilized. A comparison among the loading capacities across the range of volume flow rates reveals that there is some loss as the flow rates increase from 1– to – 5 mL min^{-1}. The decrease in capacity ranges from 7% for the lowest fiber packing density to 15% for the highest. Overall, this decrease is practically inconsequential in comparison to the improvement in throughput that would be realized in processing at 5X higher rates. As a final quantitative measure, the roles fiber packing density on the ratio q_e/q_s are presented in each table, where the individual capacities (q_e) are divided by the maximum equilibrium binding capacity of q_s = 1.30 mg g^{-1} calculated from the Moreau fit (Eq. 3.3) . As reported in the tables in Figs 3.4a–e, the highest q_e/q_s appears for the column having the fewest fibers (ε_i = 0.546) at a 1 mL min^{-1} flow rate (1.16/1.30 = 0.89). The lowest q_e/q_s appears for the column having the highest packing density at the 5 mL min^{-1} flow rate (0.87/1.30 = 0.67).

a.

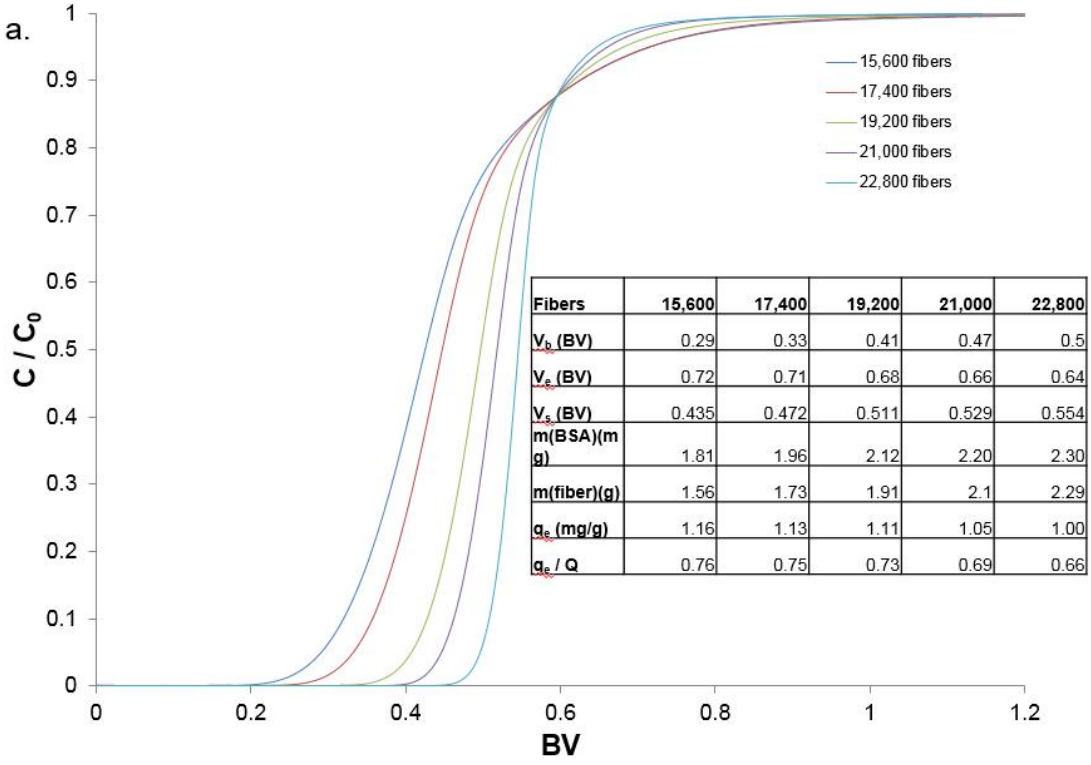

Fibers	15,600	17,400	19,200	21,000	22,800
V_b (BV)	0.29	0.33	0.41	0.47	0.5
V_e (BV)	0.72	0.71	0.68	0.66	0.64
V_s (BV)	0.435	0.472	0.511	0.529	0.554
m(BSA)(mg)	1.81	1.96	2.12	2.20	2.30
m(fiber)(g)	1.56	1.73	1.91	2.1	2.29
q_e (mg/g)	1.16	1.13	1.11	1.05	1.00
q_e / Q	0.76	0.75	0.73	0.69	0.66

b.

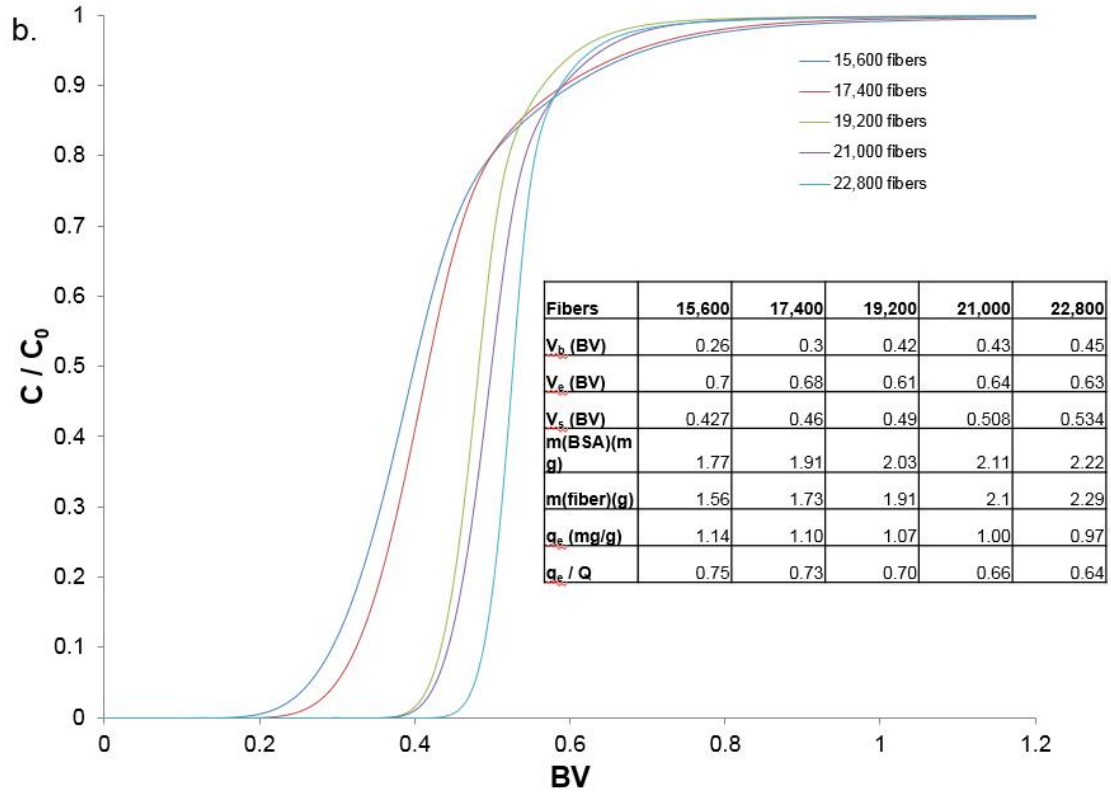

Fibers	15,600	17,400	19,200	21,000	22,800
V_b (BV)	0.26	0.3	0.42	0.43	0.45
V_e (BV)	0.7	0.68	0.61	0.64	0.63
V_s (BV)	0.427	0.46	0.49	0.508	0.534
m(BSA)(mg)	1.77	1.91	2.03	2.11	2.22
m(fiber)(g)	1.56	1.73	1.91	2.1	2.29
q_e (mg/g)	1.14	1.10	1.07	1.00	0.97
q_e / Q	0.75	0.73	0.70	0.66	0.64

c.

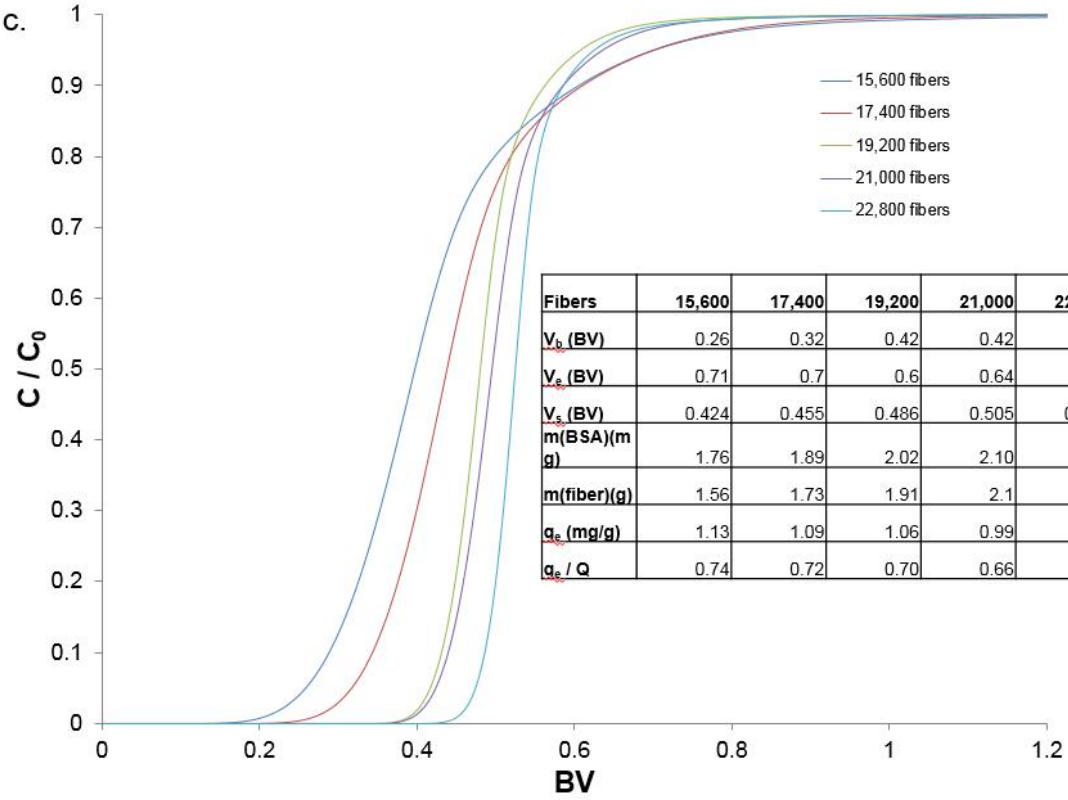

Fibers	15,600	17,400	19,200	21,000	22,800
V_b (BV)	0.26	0.32	0.42	0.42	0.48
V_e (BV)	0.71	0.7	0.6	0.64	0.63
V_s (BV)	0.424	0.455	0.486	0.505	0.531
m(BSA)(mg)	1.76	1.89	2.02	2.10	2.21
m(fiber)(g)	1.56	1.73	1.91	2.1	2.29
q_e (mg/g)	1.13	1.09	1.06	0.99	0.96
q_e / Q	0.74	0.72	0.70	0.66	0.63

d.

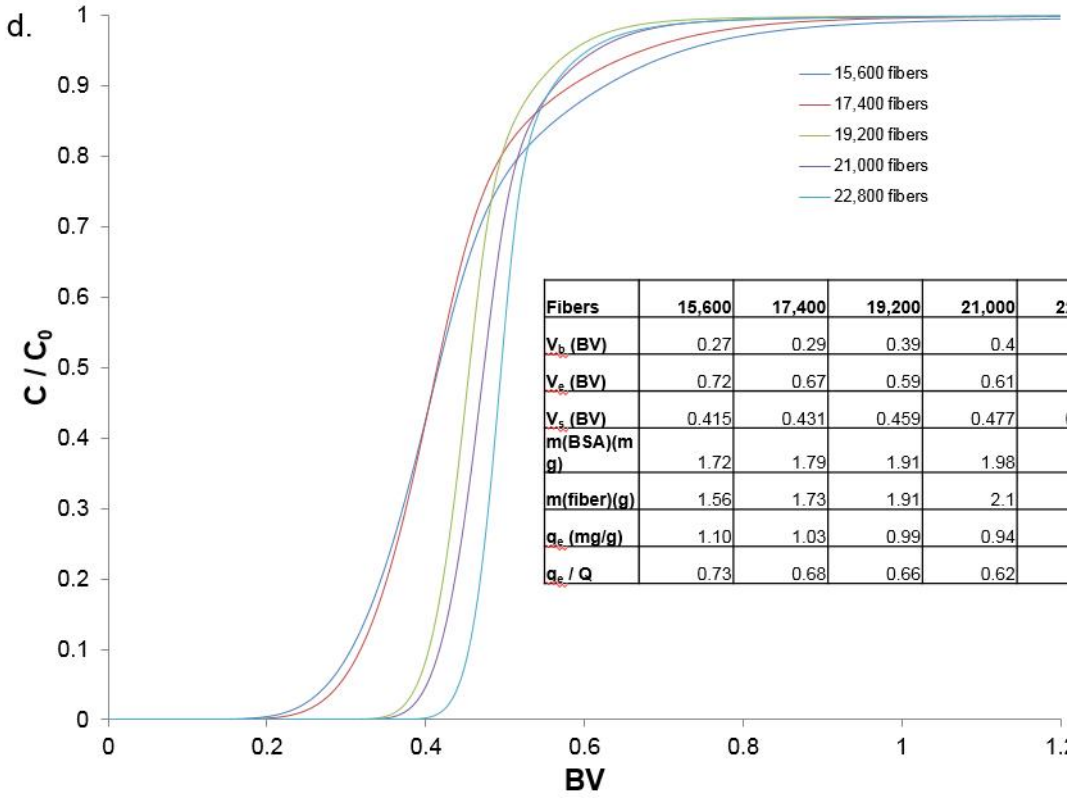

Fibers	15,600	17,400	19,200	21,000	22,800
V_b (BV)	0.27	0.29	0.39	0.4	0.44
V_e (BV)	0.72	0.67	0.59	0.61	0.6
V_s (BV)	0.415	0.431	0.459	0.477	0.501
m(BSA)(mg)	1.72	1.79	1.91	1.98	2.08
m(fiber)(g)	1.56	1.73	1.91	2.1	2.29
q_e (mg/g)	1.10	1.03	0.99	0.94	0.91
q_e / Q	0.73	0.68	0.66	0.62	0.60

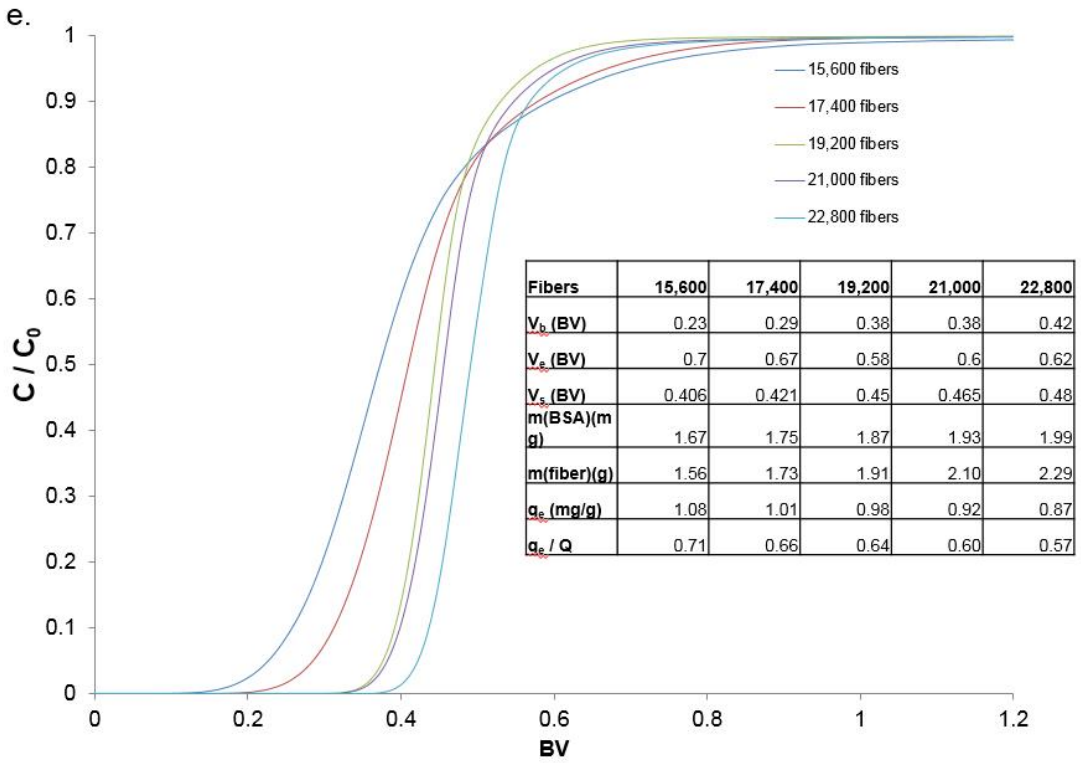

Fibers	15,600	17,400	19,200	21,000	22,800
V_b (BV)	0.23	0.29	0.38	0.38	0.42
V_e (BV)	0.7	0.67	0.58	0.6	0.62
V_s (BV)	0.406	0.421	0.45	0.465	0.48
m(BSA)(mg)	1.67	1.75	1.87	1.93	1.99
m(fiber)(g)	1.56	1.73	1.91	2.10	2.29
q_e (mg/g)	1.08	1.01	0.98	0.92	0.87
q_e / Q	0.71	0.66	0.64	0.60	0.57

Fig. 3.4. Breakthrough curves for the dynamic loading of BSA on nylon 6 C-CP fibers for columns of different fiber number density at bulk flow rates of a) 1 mL min^{-1}, b) 2 mL min^{-1}, c) 3 mL min^{-1}, d) 4 mL min^{-1}, and e) 5 mL min^{-1}. BSA concentration = 1 mg mL^{-1} in 20 mM TRIS, pH = 7.0. Each curve is the average of triplicate experiments.

Role of load linear velocity - As the dynamic adsorption of proteins onto a sorbent surface is a kinetically-limited process, it is instructive to examine the breakthrough curves depicted in Fig. 3.4 in the context of the linear velocity under which the experiments were performed for each column packing density. In this way, the concept of column residence time can be considered. The response curves of linear velocity as a function of volume flow rate were obtained using glucose oxidase at the test compound under the non-retaining solvent conditions of 90:10 ACN:H_2O, and are shown in Fig. 3.5.

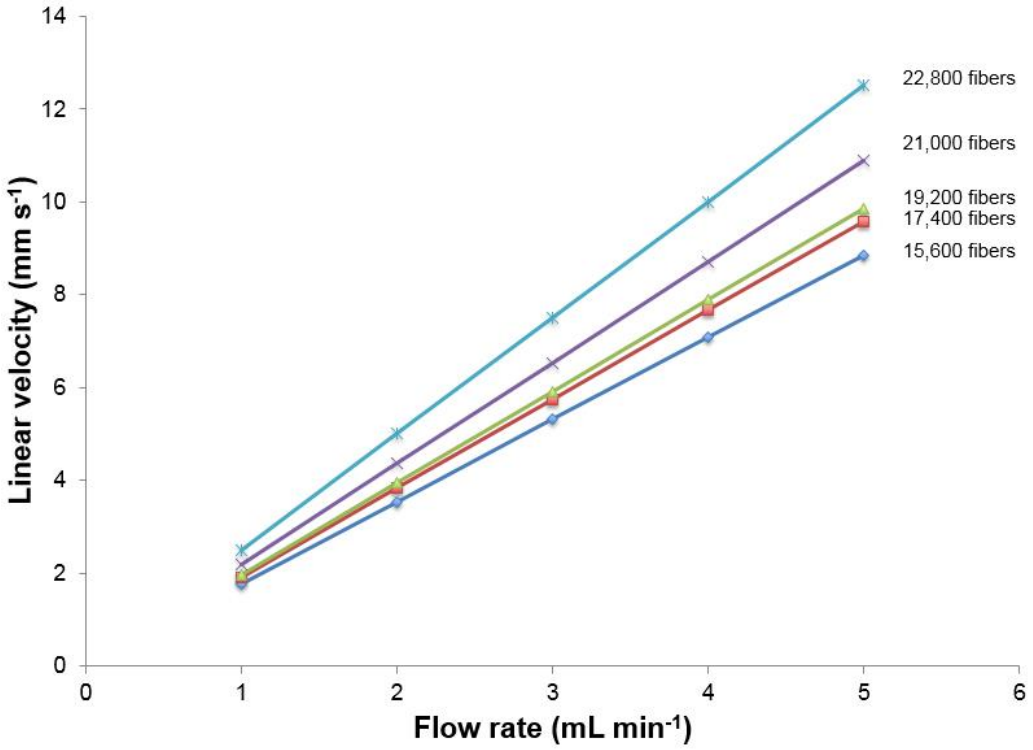

Fig. 3.5. Measured linear velocities as a function of bulk solution flow rate for 5 test columns used in the dynamic loading studies. Probe molecule = glucose oxidase in 90:10 ACN:H_2O.

As can be seen, the plots for the respective fiber packing densities are very linear. As would be expected, the slope of the lines increases with the fiber number density (inversely with the interstitial fraction). It is important to note that the linearity of the response is a validation of the respective column's physical integrity, as any compression of the bed (as with some polymer beads) would surely produce non-linear responses. In order to assess any gross kinetic limitations, Figs. 3.6a – e present the breakthrough curves for each fiber packing density along with the corresponding quantitative figures of merit. Note that these are the same curves as Fig. 3.4, but grouped for each column to isolate the roles of flow rate/velocity/residence times.

a.

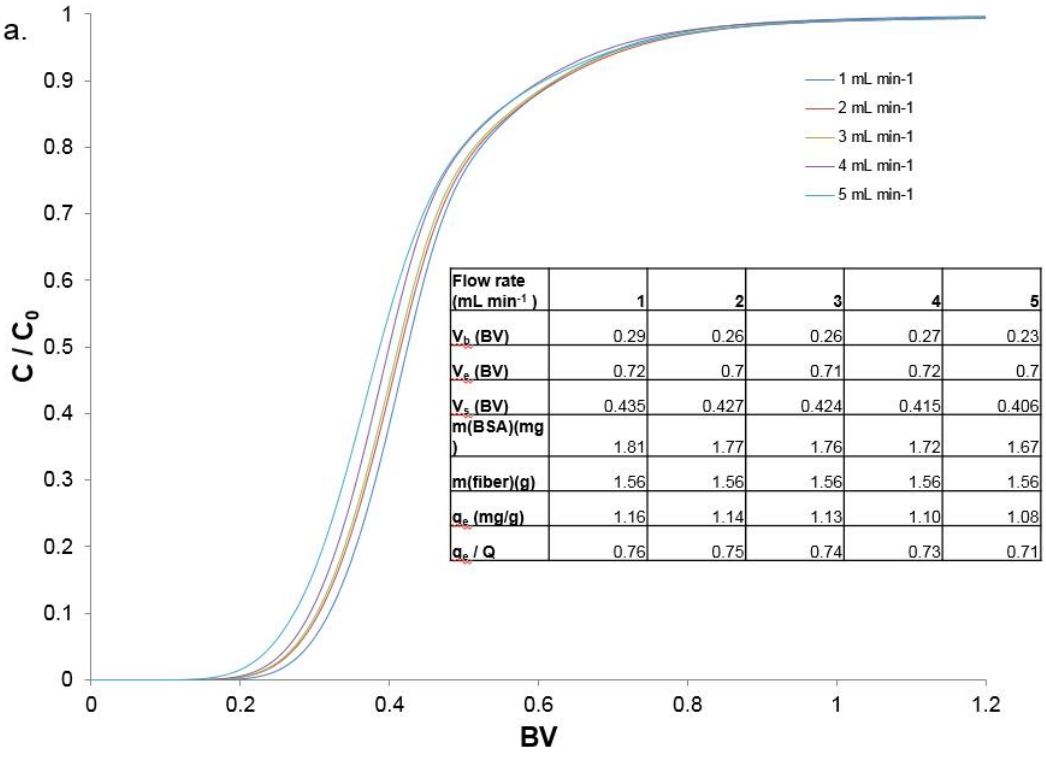

Flow rate (mL min^{-1})	1	2	3	4	5
V_b (BV)	0.29	0.26	0.26	0.27	0.23
V_e (BV)	0.72	0.7	0.71	0.72	0.7
V_s (BV)	0.435	0.427	0.424	0.415	0.406
m(BSA)(mg)	1.81	1.77	1.76	1.72	1.67
m(fiber)(g)	1.56	1.56	1.56	1.56	1.56
q_e (mg/g)	1.16	1.14	1.13	1.10	1.08
q_e / Q	0.76	0.75	0.74	0.73	0.71

b.

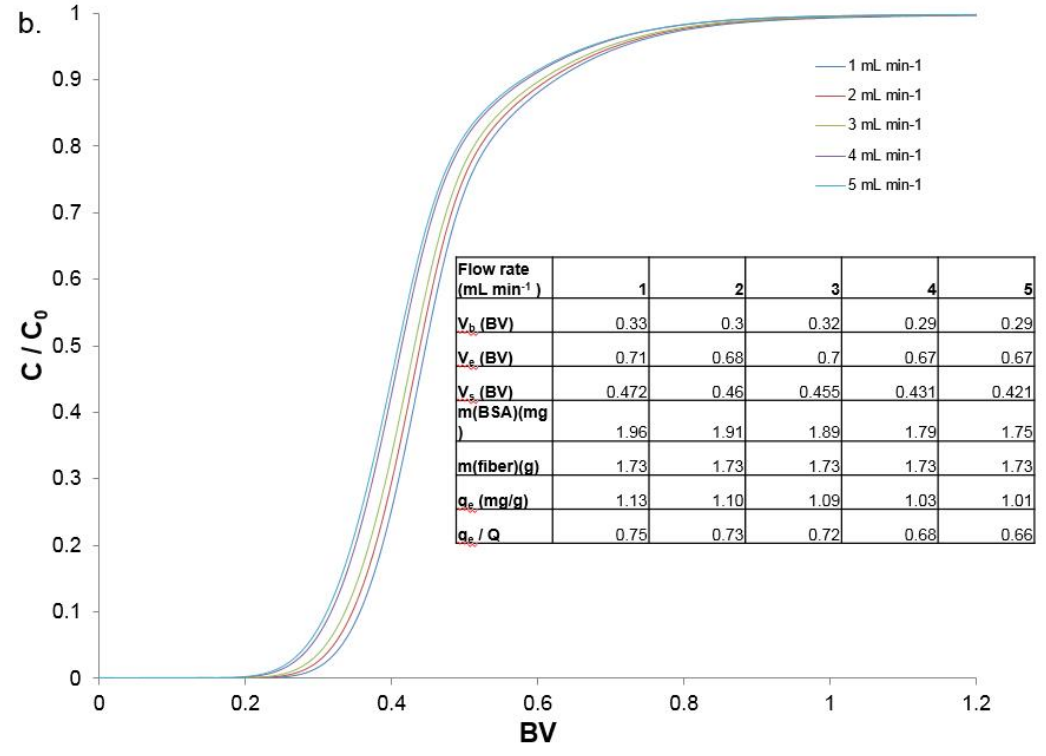

Flow rate (mL min^{-1})	1	2	3	4	5
V_b (BV)	0.33	0.3	0.32	0.29	0.29
V_e (BV)	0.71	0.68	0.7	0.67	0.67
V_s (BV)	0.472	0.46	0.455	0.431	0.421
m(BSA)(mg)	1.96	1.91	1.89	1.79	1.75
m(fiber)(g)	1.73	1.73	1.73	1.73	1.73
q_e (mg/g)	1.13	1.10	1.09	1.03	1.01
q_e / Q	0.75	0.73	0.72	0.68	0.66

c.

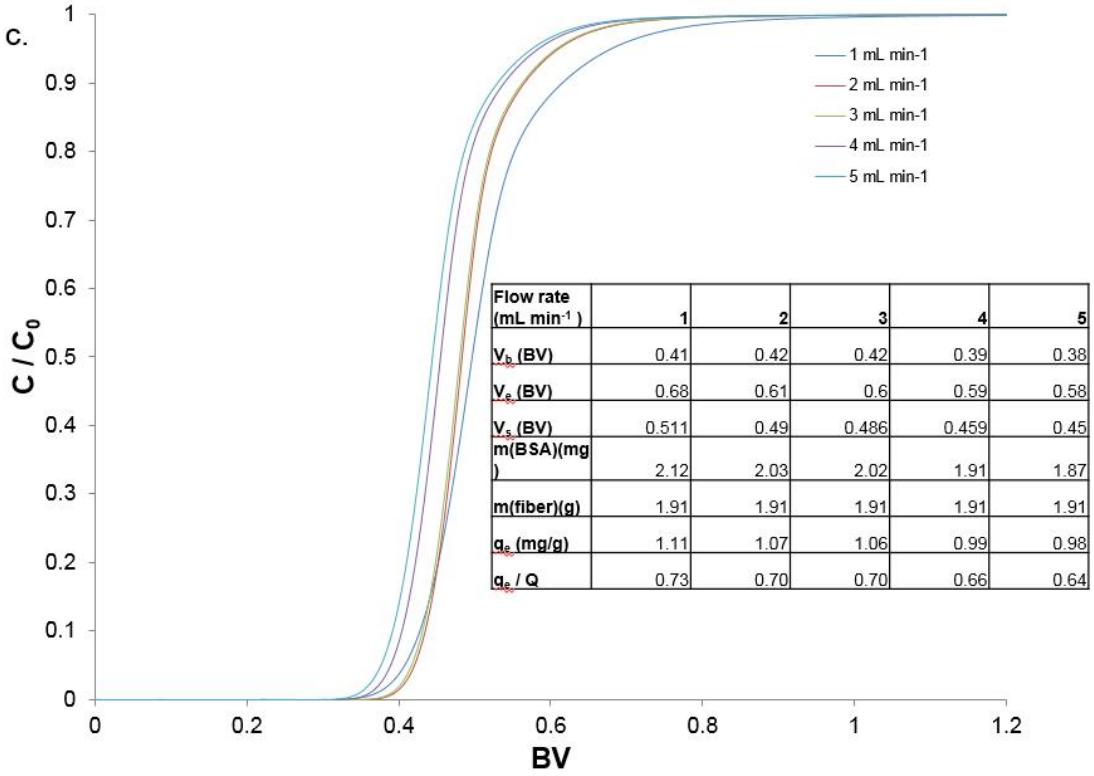

Flow rate (mL min^{-1})	1	2	3	4	5
V_b (BV)	0.41	0.42	0.42	0.39	0.38
V_e (BV)	0.68	0.61	0.6	0.59	0.58
V_s (BV)	0.511	0.49	0.486	0.459	0.45
m(BSA)(mg)	2.12	2.03	2.02	1.91	1.87
m(fiber)(g)	1.91	1.91	1.91	1.91	1.91
q_e (mg/g)	1.11	1.07	1.06	0.99	0.98
q_e / Q	0.73	0.70	0.70	0.66	0.64

d.

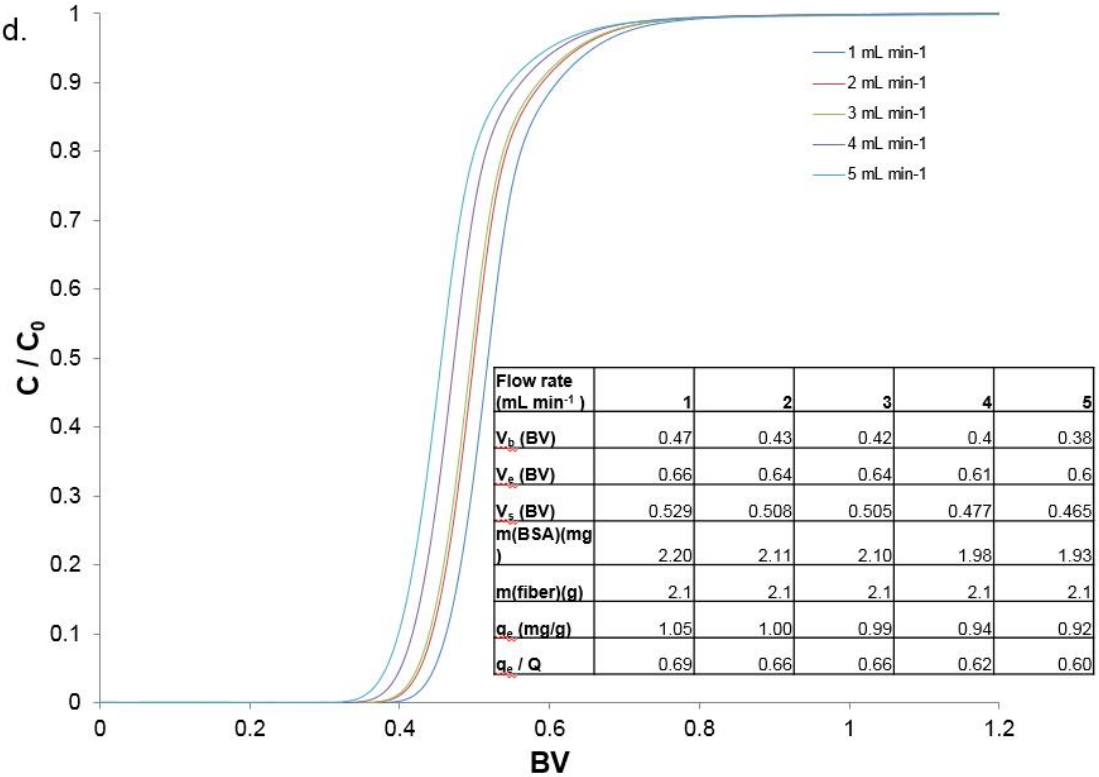

Flow rate (mL min^{-1})	1	2	3	4	5
V_b (BV)	0.47	0.43	0.42	0.4	0.38
V_e (BV)	0.66	0.64	0.64	0.61	0.6
V_s (BV)	0.529	0.508	0.505	0.477	0.465
m(BSA)(mg)	2.20	2.11	2.10	1.98	1.93
m(fiber)(g)	2.1	2.1	2.1	2.1	2.1
q_e (mg/g)	1.05	1.00	0.99	0.94	0.92
q_e / Q	0.69	0.66	0.66	0.62	0.60

ff

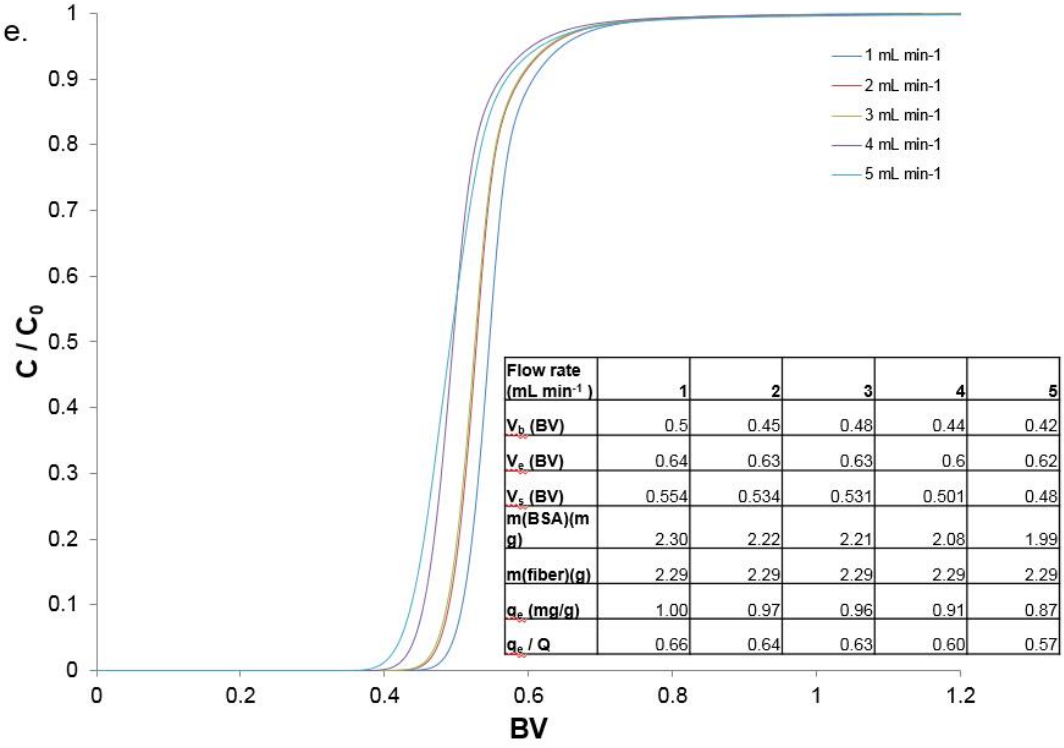

Flow rate (mL min^{-1})	1	2	3	4	5
V_b (BV)	0.5	0.45	0.48	0.44	0.42
V_e (BV)	0.64	0.63	0.63	0.6	0.62
V_s (BV)	0.554	0.534	0.531	0.501	0.48
m(BSA)(mg)	2.30	2.22	2.21	2.08	1.99
m(fiber)(g)	2.29	2.29	2.29	2.29	2.29
q_e (mg/g)	1.00	0.97	0.96	0.91	0.87
q_e / Q	0.66	0.64	0.63	0.60	0.57

Fig. 3.6. Breakthrough curves for the dynamic loading of BSA on nylon 6 C-CP fibers for different bulk flow rate/linear velocity for columns of packing densities of a) 15,600 fibers, b) 17,400 fibers, c) 19,200 fibers, d) 21,000 fibers, and e) 22,800 fibers. BSA concentration = 1 mg mL^{-1} in 20 mM TRIS, pH = 7.0. Each curve is the average of triplicate experiments.

The table entries reflect the fact that the volume flow rates are fixed at 1, 2, 3, 4, and 5 mL min^{-1}, but the different interstitial fractions yield different linear velocities. Three general trends are observed among the breakthrough curves. First, in every instance, operation at higher linear velocities yields a slight decrease in breakthrough and C/C_o = 0.5 values; reflective of decreasing amounts of adsorbed protein. It would be expected that, in the total absence of kinetic effects, the number of BV at breakthrough (V_s) for each column should not change with flow rate. Second, and consistent with Fig. 3.4., columns of low ε_i reflect slower mass transfer kinetics as evidenced by much broader transition regions of the

breakthrough curves. Finally, as the fiber packing density increases, increases in linear velocity generate steeper step functions, reflecting a situation where mass transfer rates are not limiting with linear velocity (the opposite is true for low packing densities, as would be expected).

The breakthrough curves of Fig. 3.6 suggest that there are some sacrifices in loading characteristics at high linear velocities. From a processing perspective, it is reasonable to think about the related column residence times required to saturate a bed, as this is the first component in considering the throughput of a process. On a first-principles basis, and as was demonstrated in previous sections, high fiber packing densities provide greater surface area for adsorption, and provide high mass transfer rates as the inter-fiber separation (diffusion) distances are shorter. Plotted in Fig. 3.7a are the breakthrough volumes for each of the columns as a function of the residence times (column length/linear velocity) for that set of conditions. As would be expected, for a given residence time, the column with the highest number of fibers has the largest breakthrough volume, and thus the larger amount of adsorbed protein. As expected, the amount of adsorbed protein increases as the residence time increases, with the lowest interstitial fraction column showing the greatest slope due to greater utilization of its higher binding capacity. A significant break is seen from the initial trends after the third data point for each column. Beyond this point, there is little or no advantage to providing longer exposure times. This response essentially represents the point where lower flow rates only serve to lower the overall throughput of the process

with no appreciable gain in capture capacity.

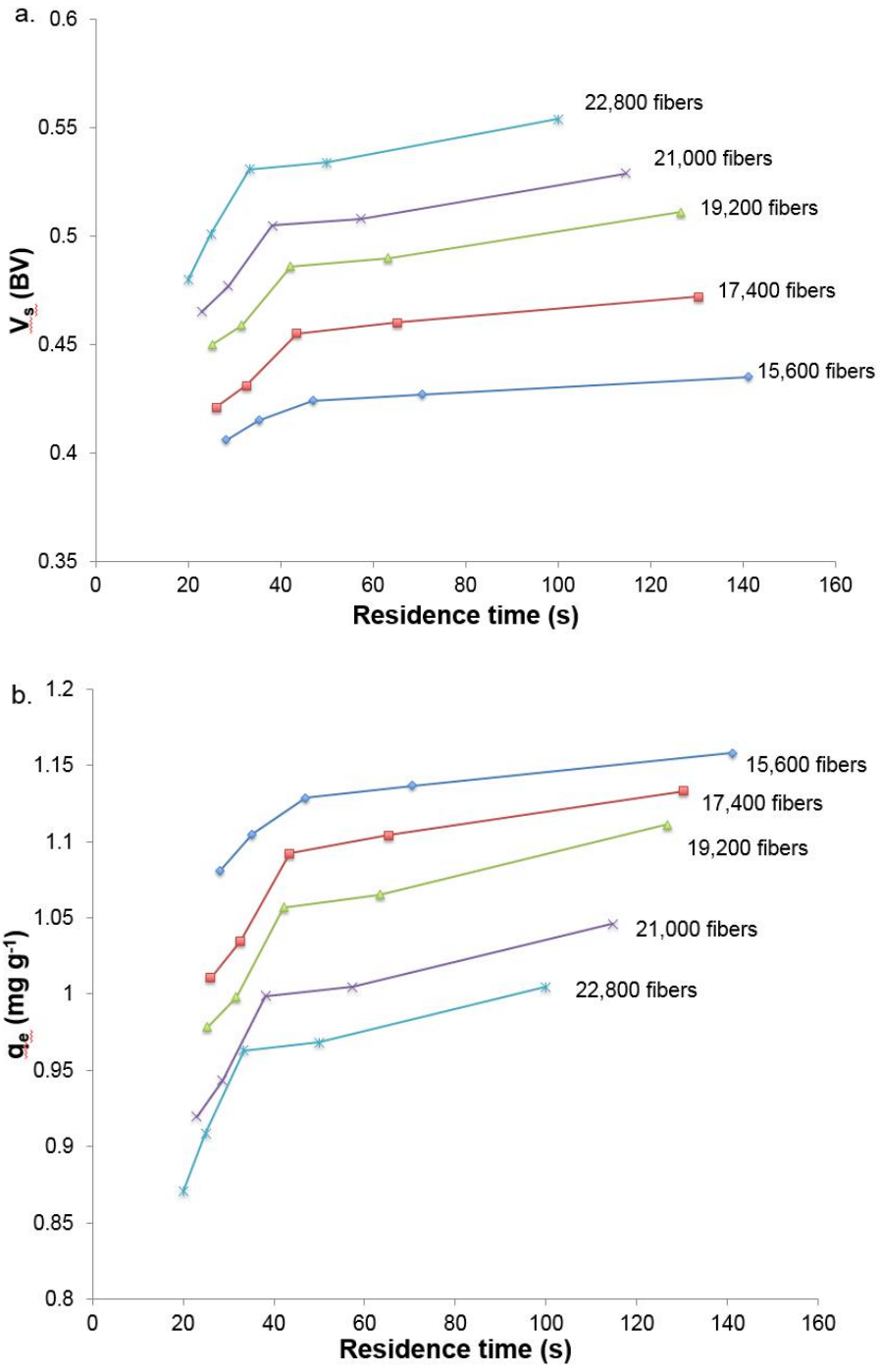

Fig. 3.7. Role of residence times (U_o/L) on the loading characteristics of nylon 6 C-CP fiber columns of different fiber number density. a) Stoichiometric volumes and b) mass-normalized binding capacities.

As suggested in previous sections, trade-offs exist in the utilization efficiency of high fiber density columns. While the absolute kinetics are rapid, those structures are not as well utilized on a per unit mass basis. This is seen more clearly as the binding capacity q_e (mg proteins per gram fiber) is plotted as a function of residence time in Fig. 3.7b. When normalizing for the bed mass of each column, it becomes clear that the fibers are more effectively loaded in the high interstitial fraction cases. Beyond the inflection point in the trendlines, the extremes in the packing densities reflect the fact that the 46% less fiber surface area of the 15,600 columns than the 22,800 columns actually lead to 16% greater binging by mass. The explanation of this is straightforward; as the fiber packing density increases, the respective fiber surfaces come into contact, and so those surfaces are not effectively wet by the load solution. So while the adsorption kinetics are faster, any surface area-based advantages are lost.

Dynamic adsorption isotherm – Having determined the optimum column packing and protein adsorption conditions in terms of q_e/q_s, it is finally important to evaluate under what protein concentrations that the processes can be performed. Dynamic loading experiments were performed over a range of protein concentrations using the column containing 15,600 nylon 6 C-CP fibers at a flow rate of 1 mL min^{-1}. The 0.1 – 1.2 mg mL^{-1} range of BSA concentrations allows direct comparison the static loading case depicted in Fig. 3.1. Figure 3.8 depicts the breakthrough curves at each BSA concentration, with each curve being representative of the average of triplicate runs. The shapes of the respective

curves are just as expected, as the higher solute concentrations show more rectangular character and the low concentrations exhibiting broader transition zones. Also as expected, the number of bed volumes required to reach the C/C_o = 0.5 point increases with decreasing protein concentration.

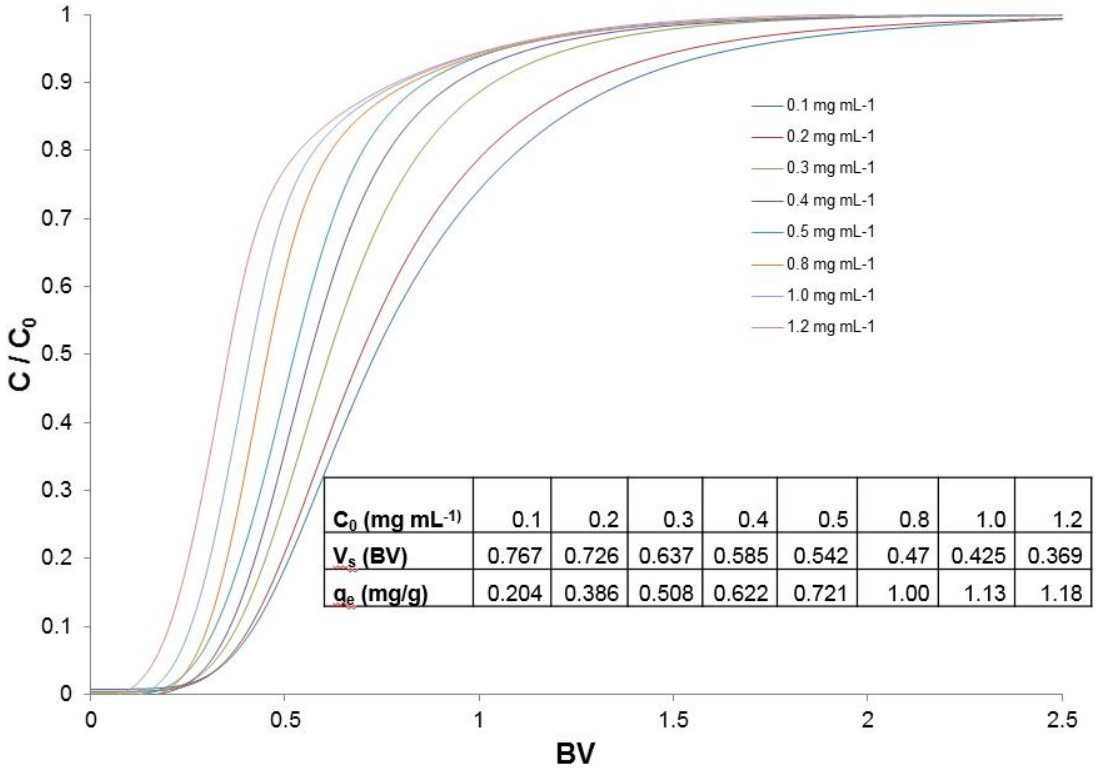

C_0 (mg mL^{-1})	0.1	0.2	0.3	0.4	0.5	0.8	1.0	1.2
V_s (BV)	0.767	0.726	0.637	0.585	0.542	0.47	0.425	0.369
q_e (mg/g)	0.204	0.386	0.508	0.622	0.721	1.00	1.13	1.18

Fig. 3.8. Breakthrough curves of BSA at concentrations of 0.1 – 1.2 mg mL^{-1} in 20 mM TRIS and the resulting quantitative binding metrics used to construct adsorption isotherms under dynamic conditions. Fiber packing density = 15,600, volume flow rate = 1 mL min^{-1}. Each curve is the average of triplicate experiments.

The tabulated results of frontal analysis of the dynamic loading experiments are included in Fig. 3.8, and plotted in the form of an isotherm in Fig. 3.9. The quantitative data were fit to the three isotherm models (Eqs. 3.1, 3.2, and 3.3) via MATLAB routines, with the resulting regression plots included in Fig. 3.9 and the

fitting parameters presented in Table 3.2.

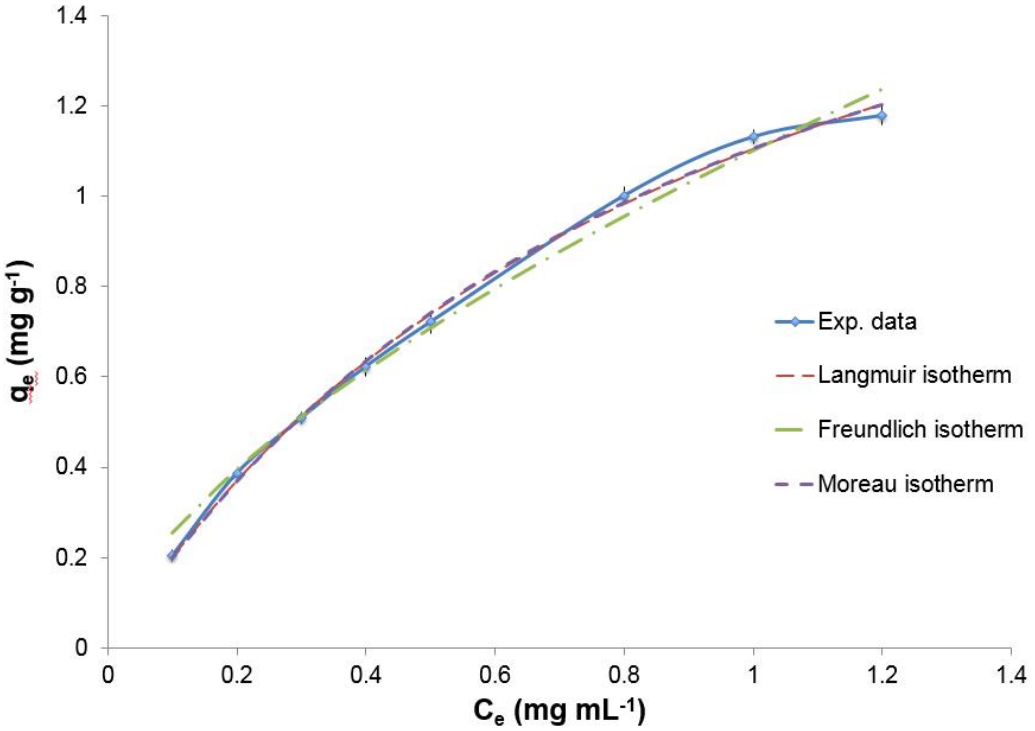

Fig. 3.9. Experimental data and regression fits for different isotherm models for the determination of the dynamic binding capacity (DBC) of BSA on nylon 6 C-CP fibers. Initial BSA concentrations = 0.1 - 1.2 mg mL^{-1} in 20 mM TRIS. Volume flow rate = 1 mL min^{-1}.

As can be seen in the figure, the fits to the experimental data are in much better agreement than for the static measurements (Fig. 3.1), with each yielding correlation coefficients of better than 0.98. Closer inspection of the derived parameters provides insight into differences in the adsorption phenomena between the static and dynamic loading situations. In the case of the Langmuir fit, an ~40% increase in the binding capacity (q_s) is observed, with a dramatic decrease in the equilibrium constant (b) reflecting a much lower dependence in the lower range of the protein concentrations. The improvement in the fit to the Langmuir model is from R^2 = 0.912 to 0.997. In the case of the Freundlich

adsorption model, very little change is seen in the binding capacity, but the surface-site homogeneity is improved substantially as the n-value is lowered from 2.8 to 1.57. Ultimately, the fit to that model improves from R^2 = 0.742 to 0.988 for the dynamic loading case. Finally, the Moreau model, which was the only one that appeared to successfully reflect the static loading situation, also shows appreciable changes in the fitting parameters while still yielding an R^2-value of 0.996. In this case, the binding capacity is seen to increase by ~60%, a much higher low-concentration binding constant (b) is revealed, and most importantly, the adsorbate-adsorbate interaction parameter decreases from I = 12,430 to 1.17. Statistically speaking, the system is best described by the Moreau isotherm model in the static mode, and the Langmuir isotherm model in the dynamic mode.

Taken as a whole, the differences in the isotherm behavior between the static and dynamic loading cases are very telling. Indeed, a *70% higher value of DBC over EBC* (2.18 vs. 1.3 mg g^{-1}) is totally counterintuitive. Because of kinetic (usually mass transfer) limitations, protein DBC values determined under practically-relevant conditions can be 5 to 10 times less than the EBCs for a given phase [61, 62]. In fact, a value of unity for DBC/EBC could only be achieved under the situation of infinitely high chromatographic efficiencies and rapid mass transfer kinetics. In the equilibrium experiments, the relatively low specific surface area of the C-CP fibers leads to low EBC values, with the high dependence at low concentrations reflecting the fact that little diffusional driving force is needed to fill the accessible surface sites. This is due to the low porosity of the fibers; only the

surface needs to be covered. On the time scale of the static experiments, proteins initially adsorbed to the surface will tend to denature. This sets up a situation wherein protein-protein interactions can cause multi-layering, as clearly indicated in the derived-parameter values and accuracy of the Moreau fit. In the case of the dynamic loading experiments, the changes in the Moreau equation I-term clearly reflect a situation wherein multi-layering is hardly existent. This is reasonable in terms of the timescale of the experiments (<3 min vs. 24 hours), with the lack of multi-layering explaining the much-improved fits to the Langmuir and Freundlich models.

As a final comparison, the increases in the calculated binding capacities under flow conditions for the Langmuir and Moreau models point to a unique situation in the case of the C-CP fiber phase. Due to the lack of porosity of the C-CP fibers, the only pertinent mass transfer process is from the bulk solution to the fiber surface, as such any physical processes which enhance this process should improve loading. The physical structure of the C-CP fiber columns, essentially a network of aligned micron-sized capillaries, provides the proper conditions to affect convective diffusion of solutes from the bulk flow to the substrate surface [23,35,63]. This happens as a consequence of the high shear rates within the column. The shear rate in a two dimensional, parallel plate system is defined as the ratio of linear velocity to the separation distance (d), $\gamma = U_o/d$. In case of C-CP fiber phases, the inter-fiber gaps are typically 1-5 μm. Thus the linear velocities depicted in Fig. 4 result in very high shear rates (400 – 14,000 s^{-1}). Under such

conditions, the concentration gradient over which diffusion from the bulk flow to the surface (i.e., the boundary layer) decreases with a $\gamma^{1/3}$ dependency (δ_c $1/\alpha$ $\gamma^{1/3}$), providing enhanced diffusion to/from the fiber surfaces [64-66]. Indeed, this phenomenon leads to the steeper slopes for the high density (shorter inter-fiber gaps) seen in high velocity region of Fig. 3.8.

In addition to higher diffusion rates, numerous studies under high shear conditions have shown that adsorbed proteins layers have very high structural uniformity, with proteins aligning somewhat vertically on the surface [67-71]. Because of the higher surface order, total binding capacities increase as well. In the case of the C-CP fiber separation of proteins, evidence for the first phenomenon has been seen through the need for lesser elution solvent strengths as the separation linear velocities increase [36,72]. The increase in the calculated DBC over the EBC for the C-CP fiber columns is thus interpreted as improved mass transport and higher degrees of surface ordering versus the static case. For this reason as well, a much broader “linear” range of the adsorption isotherm is observed.

Conclusions

The present work complements recent reports of the throughput and yield characteristics of nylon 6 C-CP fiber columns [37]. As expected, the fiber matrix shows very low equilibrium binding capacities (EBC = 1.3 mg BSA g^{-1} fiber) due to their limited porosity and thus specific surface areas. Dynamic loading

characteristics were evaluated as a function of column fiber packing density (ε_i = 0.401 – 0.546) and load linear velocity (U_o = 2 – 12.5 mm s^{-1} for flow rates of 1 – 5 mL min^{-1}) through the generation of breakthrough curves and subsequent frontal analysis. The basic structure of the breakthrough transients clearly demonstrates a number of important points. First, for a given packing density, increases in flow rate generate much steeper transitions zones; indicative of a lack of mass transfer limitations. Second, columns of lower ε_i, show sharper breakthrough curves; reflective of the shorter inter-fiber diffusion distances and thus faster adsorption rates. In terms of dynamic loading capacity, high-density packings provide greater fiber surface area per column volume, but this advantage is lost because of crimping of inter-fiber channels. Finally, and uniquely, the C-CP fiber columns actually yield improvement in capacity under dynamic loading rather than static conditions, with DBC/EBC = 1.7. Each of these characteristics is a direct result of the fiber column structure that provides high permeability (low backpressure) and yet high shear rates to affect efficient solute transport to a non-porous surface to affect adsorption.

The findings of this work, taken as tabulations based on absolute loading capacities, suffer in comparison to most commercially available phases. From the context of downstream processing, though, where throughput, yield, and the various associated costs of operation are considered [59,73], C-CP fibers are still very much worthy of further practical development. The diversity of base fiber chemistries and diverse functionalization possibilities only add to positive attributes

of the phases. Having elucidated the critical column and processing parameters, future works will focus directly on the preparative separation of immunoglobulin G (IgG) from fermentation media using a novel protein A affinity phase recently demonstrated by the simple adsorption of the protein ligand onto polypropylene C-CP fiber surfaces [74]. This effort will involve the various practical aspects of downstream processing in a way that will take advantage of the kinetic aspects of C-CP fiber separations.

References

1. E.A. Peterson, H.A. Sober, Fed. Proc., 13 (1954) 273.
2. J. Porath, P. Flodin, Nature, 183 (1959) 1657.
3. I. Mihelic, T. Koloini, A. Podgornik, A. Strancar, J. High Resolut. Chromatogr., 23 (2000) 39.
4. Y. Kato, K. Nakamura, T. Hashimoto, J. Chromatogr. A, 245 (1982) 193.
5. J.R. Mazzeo, Neue, UD, Kele, M, Plumb, RS, Anal. Chem. 77 (2005).
6. Unger, KK, Jilge, G, Kinkel, JN, Hearn, MTW. J. Chromatogr. A, 359 (1986) 61.
7. Lee, WC, J. Chromatogr. B, 699 (1997) 29.
8. Kirkland, JJ, Truszkowski, FA, Dilks, CH, Engel, GS. J. Chromatogr. A, 890 (2000) 3.
9. Gritti, F, Leonardis, I, Shock, D, Shalliker, A, Guichon, G. J. Chromatogr. A, 1217 (2010) 1589.
10. Schuster, SA, Wagner, BM, Boyes, BE, Kirkland, JJ. J. Chromatogr. A 1315 (2013) 118.
11. Ladisch, MR, Bioseparations Engineering: Principles, Practice, and

Economics. New York:Wiley-Interscience,2001.

12. Carta, G, Jungbauer, A, Protein Chromatography: Process Development and Scale-Up. Weinheim:Wiley-VCH,2010.

13. Lee, D, Svec, F, Frechet, JMJ. J. Chromatogr. A, 1051 (2004) 53.

14. Jungbauer, A, Hahn, R. J. Sep. Sci. 27 (2004) 767.

15. Jungbauer, A, Hahn, R. J. Chromatogr. A, 1184 (2008) 62.

16. Rodrigues, AE, Mata, VG, Zabka, M, Pais, L, Flow and Mass Transfer. In Monolithic Materials: Preparation, Properties, and Applications, Svec, F.; Tennikova, T. B.; Deyl, Z., Eds. Amsterdam:Elsevier Science, BV: 2003.

17. Frey, DD, Kang, XZ. J. Chromatogr. A, 16 (2005) 552.

18. Jungbauer, A.. J. Chromatogr. A, 1065 (2005) 3.

19. Ghosh, R. J. Chromatogr. A, 952 (2002) 13.

20. Kirby, RD, Cates, DM. Textile Res. J. 52 (1983) 586.

21. Yang, YQ, Velayudhan, Ladisch, MR. J. Chromatogr. A, 598 (1992) 169.

22. Hegedus, RD. J. Chromat. Sci 26 (1988) 425.

23. Hamaker, K, Liu, JY, Ladisch, MR. Biotechnol. Progr., 14 (1998) 21.

24. Singh, A, Pinto, NG. React. Polym., 24 (1995) 229.

25. Marcus, RK, Davis, WC, Knippel, BC, LaMotte, L, Hill, TA, Perahia, D, Jenkins, JD. J. Chromatogr. A, 986 (2003) 17.

26. Marcus, RK. J. Sep. Sci., 31 (2008) 1923.

27. Marcus, RK. J. Sep. Sci., 32 (2009) 695.

28. Hamaker, K, Rau, SL, Hendrickson, R, Liu, J, Ladisch, CM, Ladisch, MR. Ind. Eng. Chem. Res., 38 (1999) 865.

29. Li, CH, Ladisch, CM, Yang, YQ, Hendrickson, R, Keim, C, Mosier, N, Ladisch, MR. Biotechnol. Prog., 18 (2003) 309.

30. King, JK, Pinto, NG. J. Chromat., 609 (1992) 61.

31. Marcus, RK, Davis, WC, Knippel, BC, LaMotte, L, Hill, TA, Perahia, D, Jenkins, JD. J. Chromatogr. A, 986 (2003) 17.

32. Stanelle, RD, Marcus, RK. Anal. Bioanal. Chem., 393 (2009) 273.

33. Schadock-Hewitt, AJ, Pittman, JJ, Stevens, KA, Marcus, RK. J. Appl. Polym. Sci., 128 (2013) 1257.

34. Wang, Z, Marcus, RK. J. Chromatogr. A, 1351 (2014) 82.

35. Randunu, KM, Dimartino, S, Marcus, RK. J. Sep. Sci., 35 (2012) 3270.

36. Randunu, JM, Marcus, RK. Anal. Bioanal. Chem., 404 (2012) 721.

37. Randunu, KM, Marcus, RK. Biotechnol. Prog. 29 (2013) 1222.

38. Nelson, DM, Marcus, RK. Anal. Chem., 78 (2006) 8462.

39. Stanelle, RD, Sander, LC, Marcus, RK. J. Chromatogr. A, 1100 (2005) 68.

40. Brown, PJ, M., M, Sinclair, K, Tucker, E, Inam, A In Production, Properties and Potential Applications of Deep Groove Fiber, Southeast Regional Meeting of the American Chemical Society, 2004.

41. Guiochon, G, Shirazi, SG, Katti, AM, Fundamentals of Preparative and Nonlinear Chromatography. 2 ed.; Academic Press,2006.

42. Mollerup, JM. Chem. Eng. Technol., 31 (2008) 864.

43. Xu, X, Lenhoff, AM. J. Phys. Chem., 112 (2008) 1028.

44. Giddings, JC, Dynamics of Chromatography. New York:Marcel Dekker,1965.

45. Gritti, F, Felinger, A, Guiochon, G. Chromatographia, 60 (2004) 3.

46. Gritti, F, Guiochon, G. J. Chromatogr. A, 1069 (2005) 31.

47. Straut, CM, Marcus, RK. J. Sep. Sci., 33 (2010) 46.

48. Vera-Avila, LE, Gallegos-Perez, JL, Camacho-Frias, E. Talanta, 50 (1999).

49. Gritti, F, Guiochon, G. J. Chromatogr. A, 1099 (2005) 1.

50. Langmuir, I. J. Am. Chem. Soc., 40 (1918) 1361.

51. Freundlich, H, Z. Phys. Chemei., 57 (1906) 384.

52. Tie, Y, Calonder, C, van Tassel, PR. J. Colloid Surf. Sci., 268 (2003) 1.

53. Xu, W, Regnier, FE. J. Chromatogr. A, 828 (1998) 357.

54. Chang, C, Lenhoff, AM. 827 (1998) 281.

55. Mavropopoulos, E, Costa, AM, Costa, LT, Achete, CA, Mello, A, Granjeiro, JM, Rossi, AM. Colloids Surf. B, 83 (2011) 1.

56. Dias_cabrel, AC, Queiroz, JA, Pinto, NG. J. CHromatogr. A, 1018 (2003) 137.

57. Moreau, M, Valentin, P, Vidal-Madjar, C, Lin, BC, Guiochon, G. J. Colloid Interface Sci., 141 (1991) 127.

58. Belter, PA, Cussler, EL, Hu, W-S, Bioseparations: Downstream Processing for Biotechnology. New York:Wiley-Interscience,1988.

59. Costioli, MD, Guillemot-Potelle. C, Broly, H. Biopharm. Int., 23 (2010) 26.

60. Randunu, JM, Dimartino, S, Marcus, RK. J. Sep. Sci. 35 (2012) 3270.

61. Staby, A, Johansen, N, Wahlstrom, I. J. Chromatogr. A, 827 (1998) 311.

62. Müller, E. Chem. Eng. Technol., 28 (2005) 1295.

63. Dimartino, S, Herigstad, MO, Boi, C. J. Biotechnol., 150 (2010) 78.

64. Leveque, M. Ann. Mines, 13 (1928) 284.

65. Bird, BR, Stewart, WE, Lightfoot, EN, Transport Phenomena. New York:Wiley,1960.

66. Leal, GL, Advanced Transport Phenomena :Fluid Mechanics and Convective Transport Processes. Cambridge University Press, Cambridge,2007.

67. Dejardin, P, Vasina, EN. Colloids Surf. B, 22 (2004) 121.

68. Santore, MM. Colloid Interface Sci. 10 (2005) 176.

69. Wertz, CF, Santore, MM. Langmuir, 15 (1999) 8884.

70. Wertz, CF, Santore, MM. Langmuir, 18 (2002) 1190.

71. Wertz, CF, Santore, MM. Langmuir, 18 (2002) 706.

72. Nelson, DM, Marcus, RK. Anal. Chem., 78 (2006) 8462.

73. Nfor, BK, Zuluaga, DS, Verheijen, Biotechnol. Prog., 27 (2011) 1629.

74. Schadock-Hewitt, AJ, Marcus, RK. J. Sep. Sci., 37 (2014) 495.

CHAPTER FOUR

SUMMARY

The work in this thesis has further supported the potential of C-CP fibers as an innovative stationary phase for fast protein separations. The ultimate goal of this research is to develop the C-CP fibers to apply on fast protein separations commercially for the biotechnology and pharmaceutical industries. Chapter one overviewed the history and basic theory of HPLC, also introduced the development of protein separation techniques and stationary phases. As a stationary has advantages of rigidity, fast mass transfer, high DBC/EBC ratio, and low backpressure, C-CP fibers came into view as an excellent stationary phase for macromolecule separations.

Chapter two described the geometric structure of PP C-CP fibers by the measurement of pore size distribution on the surface. With the average pore diameter of 4.2 ± 1.1 nm / 4.0 ± 0.1 nm determined by Gaussian and log-normal distribution mode respectively, the geometric structures of C-CP fibers were better understood. This result was also verified by employing van Deemter plots, which showed negligible C-term for thyroglobulin which is totally excluded by the pores on the surface.

Chapter three described the investigation of the role of the interstitial fraction of nylon-6 C-CP fibers on protein binding capacity. The steeper transitions zones caused by increasing packing densities suggests the fast mass transfer of C-CP

fibers, and the ratio of DBC/EBC of 1.7 indicates the non-porous surface of C-CP fibers. Based on these results, C-CP fibers are well worth being further investigated in the future.

It is true that C-CP fibers still have some disadvantages, such as high plate height and low loading capacity. So the future studies will mainly focus on the modification of the surface of the fibers to improve loading capacity and decreasing the eddy diffusion to increase column efficiency. From the aspect of modification, more functional groups such as diethylaminoethyl groups (DEAE) for anion exchange chromatography, or carboxyl acid groups for cation exchange chromatography need to be introduced on the surface of the fibers to increase the loading efficiency. Additionally, the introduction of affinity ligands on the surface of fibers will increase the selectivity as chromatographic stationary phase. From the aspect of column efficiency, small size of fibers and even packing achieved from finer packing process are necessary to decrease the eddy diffusion and to increase the column efficiency.